Volcanic history reconstruction in northern Ecuador: insights for eruptive and erosion rates on the whole Ecuadorian arc

Mathilde Bablon, Xavier Quidelleur, Pablo Samaniego, Jean-Luc Le Pennec, Santiago Santamaria, Céline C. Liorzou, Silvana Hidalgo, Bastien Eschbach

Bulletin of Volcanology (2020) 82:11
https://doi.org/10.1007/s00445-019-1346-1

RESEARCH ARTICLE

Volcanic history reconstruction in northern Ecuador: insights for eruptive and erosion rates on the whole Ecuadorian arc

Mathilde Bablon[1,2] · Xavier Quidelleur[1] · Pablo Samaniego[3,4] · Jean-Luc Le Pennec[3,4] · Santiago Santamaría[1] · Céline Liorzou[5] · Silvana Hidalgo[4] · Bastien Eschbach[1]

Received: 15 March 2019 / Accepted: 27 November 2019

Abstract

In the northern Andes, the Ecuadorian arc presents a large number of Quaternary volcanoes, spread over a rather restricted area. The origin of this volcanic clustering is not well understood, and only a few chronological data older than the Holocene are available in northern Ecuador to document the arc development stages. In this study, we present new K-Ar ages obtained on lava flow and pumice samples for Cushnirumi, Mojanda, Fuya Fuya, Imbabura, Cubilche, and Cusín volcanoes, located about 40 km north of Quito, the Ecuador's capital city. Our results show that the volcanic activity in the northern part of the Ecuadorian arc started at least at ~ 1 Ma and that construction of volcanoes mainly occurred during the last 500 ka. Together with the radiometric data, numerical reconstructions of the paleomorphology of the volcanoes are used to estimate the volume of emitted magmas and the amount of eroded material in order to quantify their eruptive and erosion rates. Emission rates of Ecuadorian volcanoes range between < 0.2 and 3.6 ± 2.1 km^3/kyr. Highest rates are obtained for volcanoes constructed over time periods shorter than 100 kyr by sporadic eruptive pulses, whereas lowest rates are calculated over longer periods that include quiescence phases. Erosion rates range between 0.02 ± 0.01 and 0.14 ± 0.09 km^3/kyr and highlight that volcanic edifices whose activity ended recently are rapidly dismantled by physicochemical processes. Finally, the spatial distribution of Quaternary volcanoes as well as the spatio-temporal evolution of lava geochemistry may reflect the progressive influence of the Carnegie Ridge at depth.

Keywords Ecuador · K-Ar dating · Volcanic arc · Eruptive rates · Erosion · Volumes

Highlights

The Quaternary volcanic activity of northern Ecuador started at least at ~ 1 Ma.

Volcanoes grew during sporadic activity pulses separated by quiescence periods.

Erosion processes depend on the exposure duration and on rock weathering.

The volcanism spatial distribution may be related to the Carnegie Ridge subduction.

Eruptive rates do not seem to be linked to the plate convergence velocity.

Editorial responsibility: R. Cioni; Deputy Executive Editor: J. Tadeucci

Electronic supplementary material The online version of this article (https://doi.org/10.1007/s00445-019-1346-1) contains supplementary material, which is available to authorized users.

✉ Xavier Quidelleur
xavier.quidelleur@u-psud.fr

Mathilde Bablon
mathilde.bablon@geoazur.unice.fr

[1] GEOPS, Université Paris-Sud, CNRS, Université Paris-Saclay, Rue du Belvédère, 91405 Orsay, France

[2] Université Côte d'Azur, CNRS, IRD, Observatoire de la Côte d'Azur, Géoazur, Sophia Antipolis, 06560 Valbonne, France

[3] Laboratoire Magmas et Volcans, Université Clermont Auvergne, CNRS, IRD, OPGC, F-63000 Clermont-Ferrand, France

[4] Instituto Geofísico, Escuela Politécnica Nacional, Ladrón de Guevara E11-253, Ap, 2759 Quito, Ecuador

[5] Université de Bretagne Occidentale, Domaines Océaniques IUEM, 29280 Plouzané, France

Published online: 06 January 2020

Introduction

Detailed knowledge of the eruptive chronology of volcanoes is needed to improve volcanic hazard assessment, and to better understand the relationship between volcanic activity, geodynamics, and tectonics. However, the eruptive history of many potentially active volcanoes remains poorly documented. For instance, volcanoes, such as Chaitén (2008) in Chile, Soufrière Hills (1995) in Montserrat, or Pinatubo (1991) in the Philippines, erupted while they were considered as inactive and thus not monitored (e.g., Newhall and Solidum 2018). The Ecuadorian volcanic arc consists of more than eighty Quaternary volcanoes (Hall and Wood 1985; Barberi et al. 1988; Hall and Beate 1991; Hall et al. 2008), twenty-four of which experienced at least one eruption during the Holocene (Hall et al. 2008; Bernard and Andrade 2011; Fig. 1). Ecuador is also sheared by numerous active continental crustal faults (e.g., Tibaldi et al. 2007; Baize et al. 2015; Alvarado et al. 2014, 2016). Consequently, seismic and volcanic hazards are high in Ecuador, noticeably in the densely populated Interandean Valley.

It has been suggested that the spatial distribution of the Quaternary volcanoes of the Ecuadorian arc is related to the deep geometry of the slab and tectonics (Monzier et al. 1999; Bablon et al. 2019), with the presence of the Carnegie Ridge subducting below the Ecuadorian margin (e.g., Hall and Wood 1985; Barberi et al. 1988; Martin et al. 2014). Quaternary volcanism in Ecuador seems to start in the northern part of the arc at least at ~ 1 Ma (Samaniego et al. 2005; Hidalgo 2006; Opdyke et al. 2006; Robin et al. 2010), while volcanoes located in the southern termination are younger than ~ 600 ka (Samaniego et al. 2012; Bablon et al. 2018, 2019). The northern part of the arc coincides with the eastern prolongation of the subducting Carnegie Ridge, whose influence on both magma genesis and geochemistry of volcanic products remains debated (e.g., Gutscher et al. 1999a; Samaniego et al. 2002, 2010; Garrison and Davidson 2003; Bourdon et al. 2003; Hidalgo et al. 2007, 2012; Chiaradia et al. 2009; Robin et al. 2009).

The present study completes the geochronology data set, as well as eruptive and erosion rates, available for the northern part of the Ecuadorian arc, with the aim of improving the knowledge of the temporal and spatial evolution of the Quaternary volcanism. For that purpose, we have focused on a volcanic area north of Quito, lying above the inferred prolongation of the Carnegie Ridge (Fig. 1; Gutscher et al. 1999b). We present here, from six volcanic edifices, twenty new K-Ar ages performed on groundmass, plagioclase crystals or glass shards separated from lava flows and pumices. Combined with the numerical reconstruction of paleosurfaces and whole-rock major and trace element analyses, these ages help to better understand the relationship between arc development, magma chemistry and geodynamics, and also to

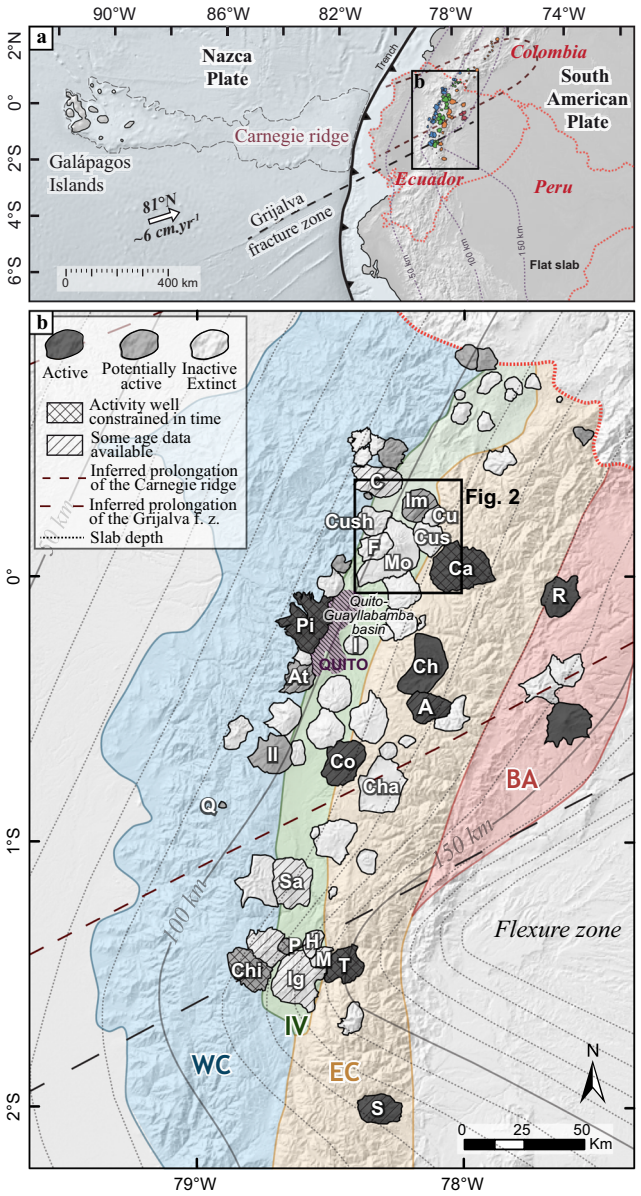

Fig. 1 **a** Geodynamic setting of Ecuador. White arrow indicates the direction of the Nazca plate motion relative to South America (DeMets et al. 2010). Dotted lines indicate the slab depth (purple; Yepes et al. 2016), the inferred prolongation of the Carnegie Ridge (brown; Gutscher et al. 1999a), and the Grijalva fracture zone (black). Ecuadorian Quaternary volcanoes are located in the Western and Eastern Cordilleras (blue and orange, respectively), in the Interandean Valley (green), and in the back-arc area (red). **b** Map of the current Ecuadorian volcanic arc. Active volcanoes (last eruption < 500 years) are represented in black, potentially active edifices (last eruption < 10 ka) in gray, and inactive or extinct Quaternary volcanoes in white (Bernard and Andrade 2011; igepn.edu.ec) WC: Western Cordillera (blue field); IV: Interandean Valley (green); EC: Eastern Cordillera (orange); BA: back-arc area (red). Notable and mentioned in text volcanoes: A: Antisana; At: Atacazo; Ca: Cayambe; Ch: Chacana; Cha: Chalupas; Chi: Chimborazo; C: Cotacachi; Co: Cotopaxi; Cu: Cubilche; Cus: Cusín; Cush: Cushnirumi; F: Fuya Fuya, H: Huisla; Ig: Igualata; I: Ilaló; Il: Iliniza; Im: Imbabura; Mo: Mojanda; M: Mulmul; Pi: Pichincha; P: Puñalica; R: Reventador; Q: Quilotoa; Sa: Sagoatoa; S: Sangay; T: Tungurahua

further investigate the role of the Carnegie Ridge on the timing of volcanism in the Ecuadorian arc.

The Ecuadorian volcanic arc

General background of the Ecuadorian Andes

The Ecuadorian Andes originate from the ongoing Late Triassic to Early Jurassic subduction of the oceanic Nazca plate beneath South America (James 1971; Aspden et al. 1987; Pindell and Kennan 2009). The oblique (~N81° E; Kendrick et al. 2003; DeMets et al. 2010) convergence velocity is currently ~ 6 cm year^{-1} (Trenkamp et al. 2002; Kendrick et al. 2003; Nocquet et al. 2014). The growth of the current volcanic arc probably started in the Mio-Pliocene in Ecuador (Barberi et al. 1988; Lavenu et al. 1992). During the Quaternary, volcanism continued north of 2° S, where the slab presents a complex subducting pattern with a flexure zone that accommodates variations of the oceanic crust thickness and change of the margin geometry (Fig. 1; Yepes et al. 2016).

The Quaternary Ecuadorian arc constitutes the southern half of the Northern Andean Volcanic Zone, which includes volcanoes from Ecuador and Colombia. Ecuadorian volcanoes are distributed along the Eastern and Western Cordilleras, in the Interandean Valley, and in the back-arc region (Fig. 1; e.g., Hall and Wood 1985; Barberi et al. 1988; Hall and Beate 1991; Hall et al. 2008). Their products are mainly calc-alkaline andesites and dacites, with some rare alkaline compositions in the back-arc (e.g., Hall et al. 2008; Hoffer et al. 2008; Hidalgo et al. 2012; Ancellin et al. 2017; Garrison et al. 2018). Time and space evolution of the arc has been studied on a regional scale (e.g., Hall and Wood 1985; Barberi et al. 1988; Hall and Beate 1991; Opdyke et al. 2006; Hidalgo et al. 2012; Ancellin et al. 2017; Bablon et al. 2019), while several studies focused on specific volcanoes (e.g., Hall et al. 1999; Robin et al. 2009; Samaniego et al. 2012). Atacazo (Hidalgo 2006), Pichincha (Robin et al. 2010), and Cayambe (Samaniego et al. 2005) volcanic complexes seem to have the oldest activity of the current arc, which began at 1.3, 1.1, and 1.1 Ma, respectively. Moreover, geochemical studies have shown that some of these volcanoes, such as Atacazo, Cayambe, Iliniza, Mojanda-Fuya Fuya, and Pichincha (Samaniego et al. 2002; Bourdon et al. 2003; Hidalgo 2006; Hidalgo et al. 2007; Robin et al. 2009; Samaniego et al. 2010), experienced geochemical changes from older typical calc-alkaline to younger adakitic signatures. The interpretation of such evolution is still debated. Garrison and Davidson (2003), Bryant et al. (2006), and Chiaradia et al. (2009) consider that the adakitic signature was acquired by assimilation or by fractional crystallization of amphibole and/or garnet-rich cumulates occurring in the thick arc crust. Alternatively, the adakitic signature could originate from the slab partial melting and the subsequent interaction of such melts with the mantle wedge (Samaniego et al. 2002, 2005, 2010; Bourdon et al. 2003; Hidalgo et al. 2007, 2012). Such scenario may be related to the increase of the slab thermal gradient induced by the subduction of the Carnegie Ridge (Fig. 1). Recently, Ancellin et al. (2017) and Narvaez et al. (2018) proposed that the subduction of the young Nazca plate and the Carnegie Ridge north of the Grijalva fracture zone (Fig. 1) could favor slab melting, while south of the Grijalva fracture zone, where the subducting plate is older, magmas mainly originate from the partial melting of the mantle wedge induced by the slab dehydration. In addition, Monzier et al. (1999) and Bablon et al. (2019) inferred that changes in the slab geometry at depth and activation of major crustal faults induced by the increase of mechanical stresses in front of the Carnegie Ridge could have favored magma genesis and rise, and a southward migration of the volcanic activity during the last ~ 600 kyr.

Northern Ecuadorian arc volcanoes

We present below a brief summary of the current knowledge of northern arc volcanoes studied here (Figs. 1b and 2), from the Western to the Eastern Cordillera.

The Mojanda-Fuya Fuya-Cushnirumi complex

About 40 km northeast of Quito, the *Mojanda-Fuya Fuya-Cushnirumi* (MFFC) volcanic complex is located in the Interandean Valley (Fig. 1) and lies upon oceanic-like Cretaceous-Paleogene volcanic formations covered by thick sedimentary deposits (Litherland et al. 1993; Jaillard et al. 2009). The ~ 20-km-wide *Mojanda* edifice (4263 m a.s.l.; Lat. 00° 07′ N; Long. 78° 16′ W) is one of the largest volcanoes of the Northern Volcanic Zone in terms of basal circumference and volume. Its morphology presents regular flanks with gentle slopes that appear similar to those of the 400–100 ka old Igualata volcano from the southern termination of the arc (Bablon et al. 2019). Mojanda volcano is made up of two edifices composed of calc-alkaline andesite lava flows with plagioclase, pyroxene, magnetite and rare amphibole, biotite or olivine crystals (Robin et al. 2009). Lower Mojanda is made of andesite and high-silica andesitic lavas and ended with the formation of a caldera, filled by basaltic andesite to andesite products of Upper Mojanda (Robin et al. 2009). Its activity ended with high magnitude phreatomagmatic eruptions, producing the summit depression presently occupied by lakes (Fig. 2b), and a ~30-m-thick regionally distributed pyroclastic sequence of ash and lapilli fallout deposits (Robin et al. 1997, 2009). This latter marks the end of the main construction of Mojanda and is covered by the Pifo pumice fallouts (Robin et al. 2009), which could have been emplaced about 165 ka (Hall and Mothes 1997) based on fission track ages of obsidian lava flows from the Chacana caldera that range between 150 ± 20 and 220 ± 20 ka (Bigazzi et al. 1992).

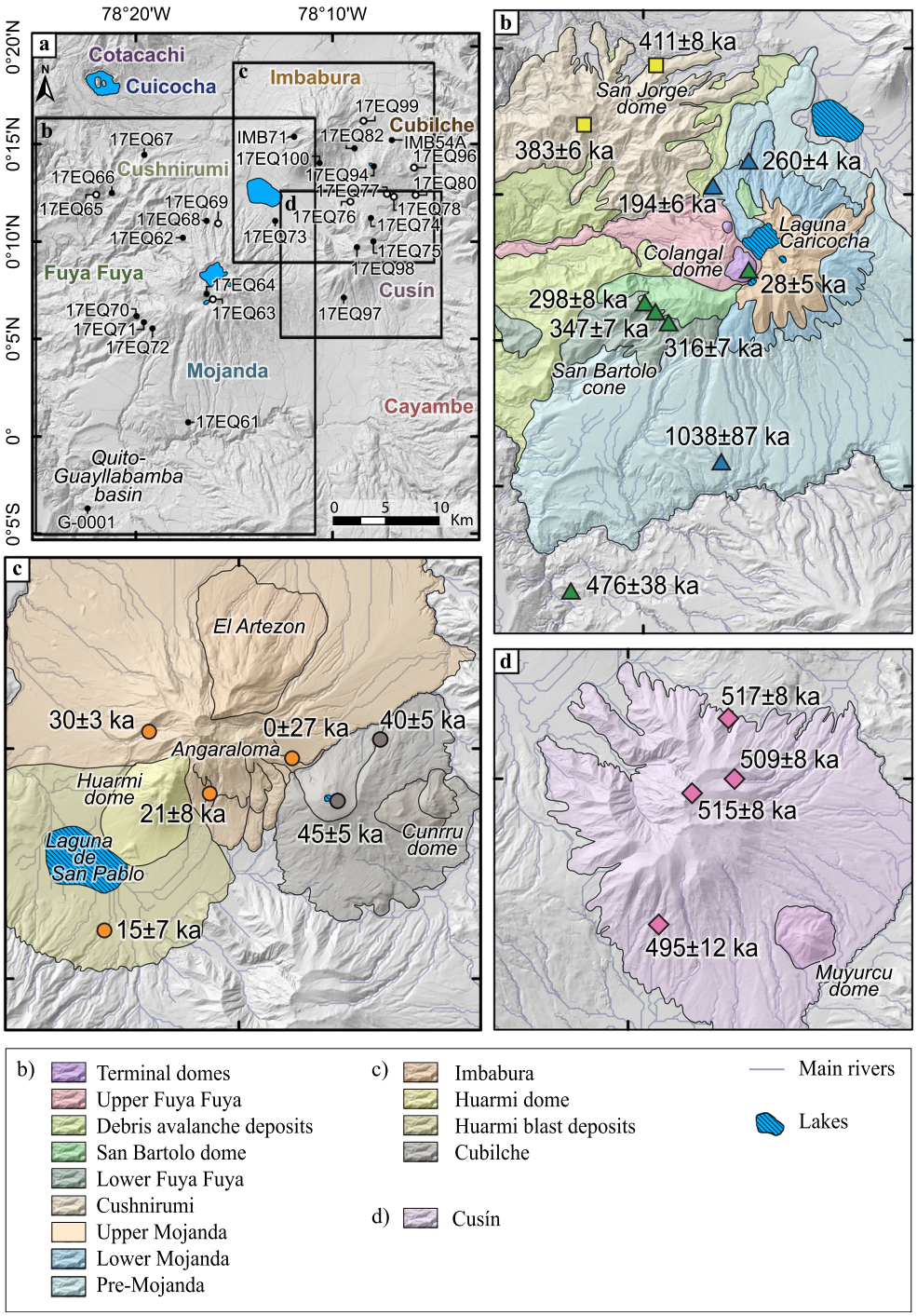

Fig. 2 **a** Shaded relief view of the SRTM Digital Elevation Model (DEM; 4-m resolution) provided by Sigtierras (http://www.sigtierras.gob.ec/) of the sampled area, with the location of all samples mentioned in this study. Samples with a white symbol have not been dated. **b**–**d** Detailed views of Mojanda-Fuya Fuya-Cushnirumi complex, Imbabura-Cubilche complex and Cusín volcanoes, respectively, with the location of our new K-Ar ages. Colored units were drawn using the geological maps of Robin et al. (2010), Le Pennec et al. (2011), and Andrade et al. (2019), for Mojanda-Fuya Fuya and Imbabura volcanoes

Fuya Fuya volcano (4279 m a.s.l.; Lat. 00° 08′ N; Long. 78° 18′ W) was constructed west of Mojanda in at least three main stages. Its activity started before the end of Lower Mojanda construction (Robin et al. 2009). The Lower Fuya Fuya activity is characterized by emplacement of viscous andesite lava flows and extrusion of dacite domes, associated with block-and-ash flow deposits, interbedded with pyroclastic flows and rhyolitic fallout deposits of plinian eruptions, mainly represented by the 3–4-m-thick "R1" and "R2" layers (Robin et al. 1997, 2009). The second construction stage of Fuya Fuya was prevalently effusive, and corresponds to the construction of the San Bartolo andesitic cone (Fig. 2b). This stage was contemporaneous with the last period of Upper Mojanda activity, and ended with a sector collapse that affected the San Bartolo cone and the southwestern flanks of Lower Fuya Fuya and Mojanda edifices (Robin et al. 2009). The resulting amphitheater was then filled by andesite to dacite lava flows and dome extrusions that constitute the Upper Fuya Fuya sequence. The Panecillo and Colangal summit domes

lack glacial erosion (Robin et al. 2009) and could have been emplaced after the Last Glacial Maximum (LGM; 30–14 ka; Clapperton 1990). Few geochronological data are available to constrain the period of construction of both volcanoes, since there is only one whole-rock K-Ar age of 590 ± 60 ka (Barberi et al. 1988), obtained for a lava flow from Mojanda, whose location is not available. *Cushnirumi* volcano (3776 m a.s.l.; Lat. 00° 11′ N; Long. 78° 20′ W) is located northwest of the Mojanda-Fuya Fuya edifices, on the eastern edge of the Western Cordillera. Only a curved ridge remains from this edifice (Fig. 2b) highly dismantled by erosion and a sector collapse that could have destroyed its southern flank (Robin et al. 1997). The collapse probably occurred before the construction of Upper Fuya Fuya, since the floor of the resulting amphitheater is covered by the debris avalanche deposits of the San Bartolo cone (Robin et al. 2009).

Imbabura and Cubilche volcanoes

North-northeast of the MFFC complex, *Imbabura* volcano (4621 m a.s.l.; Lat. 00° 16′ N; Long. 78° 11′ W; Fig. 2c) has a characteristic concave downward profile with steep flanks incised by deep glacial valleys in its upper part. This volcano is made up of two edifices and experienced at least one major northward-directed sector collapse (Ruiz 2003; Le Pennec et al. 2011; Andrade et al. 2019), whose scars were erased by erosion or covered by younger products from the terminal edifice, which includes the current summit complex called Taita Imbabura. The oldest $^{40}Ar/^{39}Ar$ age obtained for this edifice is 47 ± 6 ka (Le Pennec et al. 2011). The construction of the older Imbabura edifice was characterized by the emission of andesitic lava flows containing plagioclase, pyroxene, amphibole, Fe-Ti oxides, and accessory olivine phenocrysts, followed by an explosive activity and the generation of block-and-ash flows about 35 ka (Le Pennec et al. 2011). The southwestern flank experienced a small sector collapse about 30 ka, immediately followed by a lateral blast (Fig. 2c) and construction of the Huarmi Imbabura dome complex (Le Pennec et al. 2011). Activity of Taita Imbabura resumed with the construction of the El Artezon dome on its northern flank, and has continued until Early Holocene times (Ruiz 2003; Le Pennec et al. 2011) with the emplacement of block-and-ash flows, as well as thick lava flows on the southeastern flank (Fig. 2c). *Cubilche* volcano (3828 m a.s.l.; Lat. 00° 14′ N; Long. 78° 08′ W) is located southeast of Imbabura. Lava flows from both Imbabura and Cubilche volcanoes range from low silica andesites to dacites and belong to the medium-K calc-alkaline series. The mineralogy mainly consists of tabular plagioclase, clino-orthopyroxene and destabilized amphibole crystals, and accessory minerals such as Fe-Ti oxides and olivine (Andrade 2009; Le Pennec et al. 2011). Although no geochronological data are available, Hall and Beate (1991) proposed that this volcano results from an eastern migration of Imbabura activity, while, based on rock composition data, Andrade (2009) suggested that both Cubilche and Imbabura volcanoes are fed by the same magmatic system. The northern flank of Cubilche collapsed (Fig. 2c; Roverato et al. 2018), followed by the construction of a younger cone within the resulting amphitheater. As block-and-ash flows from Imbabura dated at ~ 9 ka cal BP (Le Pennec et al. 2011) lie upon the avalanche scar and post-collapse lava flows from Cubilche, the Cubilche collapse occurred before 9 ka. The well-preserved Cunrru dome complex (also called Cunro; Hall and Beate 1991; Fig. 2c) lies on the eastern flank of the volcano.

Cusín volcano

South of Imbabura and Cubilche volcanoes, *Cusín* volcano (3989 m a.s.l.; Lat. 00° 10′ N; Long. 78° 09′ W) is an andesitic heavily eroded edifice, whose morphology is characterized by a straight corridor with a flat floor towards the northwest (Fig. 2d). No geochronological nor geochemical data are available for this edifice. However, since the Imbabura blast deposits crop out at the foot of its western flank (Fig. 2c), the construction of Cusín should have ended before ~ 29 ka (calibrated ^{14}C determinations; Le Pennec et al. 2011), and its morphology has therefore been carved by the glacial erosion associated with the LGM.

Cayambe volcano

Cayambe volcano (5790 m a.s.l.; Lat. 00° 01′ N; Long. 77° 59′ W), located in the Eastern Cordillera (Figs. 1 and 2a), is one of the highest Ecuadorian volcanoes and is still considered active. The volcano was constructed in two stages, separated by a ~ 600 ka quiescence period (Samaniego et al. 2005). Viejo Cayambe volcano was active between 1.1 and 1.0 Ma, whereas the Nevado Cayambe activity onsets at ~ 400 ka (Samaniego et al. 1998, 2005).

Construction and destruction processes of volcanoes

During their history, volcanoes experienced alternating periods of construction and destruction. Eruptive rates correspond to the volume of volcanic products emitted over a given time period, and allow to investigate magmatic processes, and to improve hazard assessments and forecasts of eruptive dynamics. Construction of arc volcanoes occurs during sporadic activity phases characterized by high eruptive rates, separated by quiescence periods of variable duration (e.g., Hildreth and Lanphere 1994; Samaniego et al. 2016; Grosse et al. 2018). Erosion results from weathering of surface rocks by chemical or physical processes. The weathering rate depends on the climatic conditions and the nature of the exposed rock (Meybeck 1987; Bluth and Kump 1994), and is higher in tropical and equatorial regions, where rainfall and temperature

are high and where the soil is covered by a luxurious vegetation (e.g., Gaillardet et al. 1999; Ruddiman 2001; Rad et al. 2011). Physical weathering is a mechanical process that breaks down rocks into smaller fragments and particles, by volume variation during temperature changes, eolian weathering processes, mass wasting, collapse events, or during glacial abrasion. These processes dominate in cold and dry areas (Hallet et al. 1996). As physical weathering favors water circulation and increases the surface area of the particles, it accelerates chemical weathering. Consequently, each type of weathering favors the other (e.g., Louvat and Allègre 1997; Gaillardet et al. 1999; Rad et al. 2013). We will thus refer to physicochemical erosion further on. In volcanic context, erosion is favored by several processes, such as rapid construction of the volcano, deposition of unconsolidated material, as well as steep slopes (Karátson et al. 2012). Erosion affects the volcano flanks until they reach their equilibrium profile, and erosion rates are therefore related to the exposure duration (e.g., Taylor and Blum 1995; Karátson et al. 2012; Rad et al. 2013).

In Ecuador, eruptive and erosion rates are poorly documented. Eruptive rates calculated for Pichincha, Chimborazo, and Tungurahua volcanoes (Fig. 1) range between 0.1 and 2.5 km^3/kyr, and highlight that the highest rates are obtained for construction phases that occurred over short time periods compared to the lifespan of these edifices (Robin et al. 2010; Samaniego et al. 2012; Bablon et al. 2018). Data on erosion rate are rare, and only the rate of 0.2 ± 0.1 km^3/kyr, obtained for the oldest stage of Tungurahua volcano, is available (Bablon et al. 2018).

Materials and methods

K-Ar dating and geochemical analysis procedures

Twenty-nine lava flows, pumice fallouts, and juvenile blocks of pyroclastic flow deposits from Mojanda, Fuya Fuya, Cushnirumi, Imbabura, Cubilche, and Cusín volcanoes were sampled during field campaigns between 2013 and 2017 (Fig. 2a), with the purpose of sampling oldest and youngest units of each volcano, whenever possible, to constrain their activity periods. Twenty samples, selected for their freshness and low vesicle content (thin sections are shown in ESM 1), were dated using the potassium-argon (K-Ar) method with the unspiked Cassignol-Gillot technique (Cassignol and Gillot 1982). This technique is well suited for Quaternary volcanic products, which contain low radiogenic argon ($^{40}Ar^*$; Gillot et al. 2006). It has been successfully applied to Ecuadorian volcanoes (Bablon et al. 2018, 2019), as well as in other subduction zones worldwide (e.g., Samper et al. 2009; Germa et al. 2010, 2011; Ricci et al. 2015b; Grosse et al. 2018). Description of the method rationale, sample preparation, analytical procedures, standards used, and uncertainties calculation are provided in Bablon et al. (2018). Both potassium and argon measurements were performed on the separated groundmass for lava flows and for the juvenile block of pyroclastic flow deposit of Fuya Fuya volcano (17EQ71), on plagioclase crystals for the juvenile block of the Huarmi Imbabura blast deposit (17EQ73), or on the glass shards for the pumice fallout sample of Fuya Fuya volcano (G-0001; Fig. 2a). These measurements were carried out at the GEOPS laboratory at Orsay (Paris-Sud University, France), and were performed at least twice to check their reproducibility within their uncertainty range, given at the 1-σ confidence level. Results are provided in Table 1.

Whole-rock major and trace element contents of all samples are available in ESM 2. They were measured at the Laboratoire Géosciences Océan of the Université de Bretagne Occidentale (Brest, France) by ICP-AES (Inductively Coupled Plasma-Atomic Emission Spectrometry), following the procedure detailed in Cotten et al. (1995). Only for samples IMB54A and IMB71, major elements were measured at the Laboratoire Magmas et Volcans (Clermont-Ferrand, France). Relative uncertainties are $\leq 2\%$ for major elements and $\leq 5\%$ for trace elements.

Sampling

Twelve lava flows were sampled in the *Mojanda-Fuya Fuya-Cushnirumi complex*. Sample 17EQ61 is from a columnar jointed lava flow located at the southern foot of Mojanda. It lies on the sedimentary filling of the Guayllabamba basin (Fig. 2a), and, based on its stratigraphic position, corresponds to the oldest activity of Mojanda. Sample 17EQ62 is a massive lava flow that belong to the upper part of Lower Mojanda (Robin et al. 2009; Fig. 2a, b). Samples 17EQ68 and 17EQ69 are distal autobrecciated lava flows from the northern flank of Lower Mojanda. Sample 17EQ63 is a summit lava from Upper Mojanda (Fig. 2b). Samples 17EQ70 and 17EQ72 belong to the San Bartolo unit of Fuya Fuya (green unit; Fig. 2b). 17EQ71 is a juvenile block from a pyroclastic flow deposit covered by the lava flow of 17EQ70, and belongs to the upper part of Lower Fuya Fuya. Sample 17EQ64 corresponds to a summit lava flow from the Colangal terminal dome of Upper Fuya Fuya (Fig. 2b). Both 17EQ65 and 17EQ66 are proximal lava flows located in the summit area of Cushnirumi volcano, while 17EQ67 is a northern distal lava flow, mapped as San Jorge dome (Fig. 2b; Robin et al. 2009). We also sampled a pumice fallout deposit in the Guayllabamba basin (G-0001; Fig. 2a), which may correspond to the R2 fallout deposit that has been emplaced during the Lower Fuya Fuya plinian activity (Robin et al. 2009).

As the recent activity of *Imbabura* volcano has already been reconstructed by ^{14}C ages (Le Pennec et al. 2011), we focused on its older units. Samples IMB71 and 17EQ82 are lava flows from the western and eastern flanks, respectively. Sample 17EQ100 is from the distal part of the southeastern

Table 1 K-Ar ages obtained in this study. All ages were measured on separated groundmass, except those marked with asterisks, that were carried out on plagioclase crystals (*) or on pumice glass shards (**). Column headings indicate sample name, outcrop location and the corresponding eruptive stage, sample coordinates projected using the Universal Transverse Mercator (UTM) coordinate system (Zone 17), potassium content in percent, radiogenic argon content in percent and atoms per gram, age obtained for each measurement, and weighted mean age in ka, given with 1-σ uncertainty. FF: Fuya Fuya

Sample	Location and description	Longitude (m)	Latitude (m)	K (%)	^{40}Ar* (%)	^{40}Ar* × 10^{11} (at/g)	Age ± 1σ (ka)	Mean age (ka)
Cushnirumi volcano								
17EQ67	Distal lava flow, NE flank	797,677	10,026,602	1.382	8.5	5.9784	414 ± 8	411 ± 8
					6.4	5.8658	406 ± 9	
17EQ65	Proximal lava flow, summit part	793,134	10,022,847	1.411	20.6	5.6981	387 ± 6	383 ± 6
					22.4	5.5799	379 ± 6	
Fuya Fuya volcano								
G-0001	Distal pumice fallout deposit from Lower Fuya Fuya	792,301	9,993,157	2.018	1.1	10.126	480 ± 43**	476 ± 38**
					1.4	9.9617	473 ± 34**	
17EQ71	Juvenile block from a pyroclastic flow deposit, SW flank, Lower Fuya Fuya	797,608	10,010,801	1.559	8.4	5.6870	349 ± 6	347 ± 7
					5.0	5.5963	344 ± 8	
17EQ72	Lava flow, SW flank, San Bartolo unit	798,438	10,010,195	1.734	5.1	5.8031	320 ± 8	316 ± 7
					5.4	5.6547	312 ± 7	
17EQ70	Lava flow, SW flank, San Bartolo unit	796,935	10,011,374	1.291	4.0	4.0595	301 ± 9	298 ± 8
					4.7	3.9734	295 ± 8	
17EQ64	Summit lava flow from the Colangal terminal dome of Upper Fuya Fuya	803,556	10,013,449	1.687	0.6	0.5022	29 ± 5	28 ± 5
					0.5	0.4769	27 ± 5	
Mojanda volcano								
17EQ61	Distal lava flow, S flank, "pre-Mojanda" unit	801,800	10,001,323	1.702	1.4	18.523	1042 ± 78	1038 ± 87
					1.1	18.379	1034 ± 97	
17EQ68	Distal autobrecciated lava flow, N flank, Lower Mojanda	803,543	10,020,365	2.332	10.2	6.3479	261 ± 4	260 ± 4
					12.2	6.3045	259 ± 4	
17EQ62	Massive lava flow, NNW flank, upper part of Lower Mojanda	801,286	10,018,766	1.987	3.9	4.0450	195 ± 6	194 ± 6
					4.1	3.9988	193 ± 5	
Imbabura volcano								
IMB71	Lava flow, SW flank	811,806	10,028,317	1.052	1.0	0.3396	31 ± 3	30 ± 3
					0.9	0.3241	29 ± 3	
17EQ100	Lava flow, S flank, Angaraloma unit	814,241	10,025,832	1.232	0.3	0.3205	25 ± 8	21 ± 8
					0.2	0.2122	19 ± 8	
					0.3	0.2475	16 ± 7	
17EQ82	Lava flow that partly cover the collapse scar of Cubilche, E flank	817,527	10,027,245	1.212	< 0.1	− 0.0075	− 1 ± 25	0 ± 27
					< 0.1	0.0034	0 ± 28	
17EQ73	Fresh and juvenile block from the blast deposit of the Huarmi dome	810,022	10,020,360	0.821	0.2	0.1328	15 ± 7*	15 ± 7*
					0.2	0.1173	14 ± 7*	
Cubilche volcano								
17EQ94	Summit lava flow from the post-collapse edifice	819,350	10,025,548	1.006	1.0	0.4905	47 ± 5	45 ± 5
					0.8	0.4480	43 ± 5	
IMB54A	Lava flow from the northeastern edge of the scar that belongs to the pre-collapse edifice	821,064	10,028,009	1.075	0.9	0.4518	40 ± 4	40 ± 5
					0.7	0.4348	39 ± 5	
Cusín volcano								
17EQ74	Distal lava flow, N flank	819,076	10,020,622	1.366	18.9	7.4582	523 ± 8	517 ± 8
					14.7	7.2684	509 ± 8	
17EQ98	Summit vitreous lava flow	817,756	10,017,890	2.733	11.7	14.914	522 ± 9	515 ± 8
					14.6	14.526	509 ± 8	
17EQ75	Proximal lava flow near a waterfall, NE flank	819,302	10,018,413	1.313	14.5	7.0068	511 ± 8	509 ± 8
					15.1	6.9469	506 ± 8	
17EQ97	Distal lava flow, S flank	816,533	10,013,110	1.257	4.6	6.5152	496 ± 13	495 ± 12
					5.0	6.4898	494 ± 12	

lava flow sequence of Angaraloma unit, and corresponds to a reawakening of Imbabura activity during, or following, the construction of the Huarmi Imbabura dome (Le Pennec et al. 2011; Andrade et al. 2019). Unfortunately, we were unable to sample a proximal lava flow of the southeastern flank, due to the strong alteration of all outcrops. 17EQ99 is a juvenile block from a pyroclastic flow deposit from the northeast flank, which may have been emplaced between ~ 30 and 8 ka (Le Pennec et al. 2011). This deposit, as well as the lava flow of 17EQ82 whose levees are still preserved, partly cover the collapse scar of Cubilche, and are therefore younger than the avalanche event. We also sampled a fresh and juvenile block from the Huarmi blast deposit (17EQ73), which crops out in the northern foot of Mojanda volcano (Fig. 2c).

Seven rocks were sampled from *Cubilche* volcano. Sample IMB54A is from a lava flow from the northeastern edge of the scar (Fig. 2a, c) that belongs to the pre-collapse edifice, and 17EQ94 is a summit lava flow from the post-collapse cone. Samples 17EQ76, 17EQ77, 17EQ78, and 17EQ80 are distal terminations of lava flows located in the southern foot of the pre-collapse edifice, and 17EQ96 is from a massive block that crops out on the top of the Cunrru cone (Fig. 2a).

Finally, we sampled four lava flows from *Cusín* volcano. Samples 17EQ74 and 17EQ97 are distal lava flows, from the northern and the southern flanks, respectively. Sample 17EQ75 is a proximal lava flow from the eastern flank, and 17EQ98 is a glassy lava flow from the summit, which may represent the last activity of Cusín.

Numerical reconstructions of paleomorphologies

Although basal surface of volcanoes can be roughly used as a proxy for their volume (Grosse et al. 2009), the numerical reconstruction of the paleomorphology of each volcano allows us to approximate the volume of proximal material emitted during the construction of the volcanic edifices. Furthermore, it is also possible to calculate the volume of eroded products since their last activity. Considering the duration of activity and quiescence periods for each volcano, we can then quantify their output and erosion rates, respectively.

The surface elevation models prior to the construction of the edifices were obtained using a kriging interpolation method with ArcGIS software, based on the present basement elevation around the volcanoes extracted from a 90-m SRTM Digital Elevation Model (DEM). Since it is not possible to precisely know the topography below each volcano before their construction, it should be kept in mind that this may introduce an error to the volume calculation. The surface elevation model of each edifice at the end of their construction was extrapolated using the present elevation data that are considered as non-eroded, such as crests or smooth plateaus (e.g., Germa et al. 2015; Ricci et al. 2015a; Bablon et al. 2018). The constructed volume then corresponds to the difference between the modeled surface at the end of the construction and the extrapolated basement topography, whereas the eroded volume corresponds to the difference between the modeled surface before the erosion and the present elevation of the volcano. Consequently, the bulk output rate corresponds to the volume of proximal material emitted during the construction period of the volcano, whereas the erosion rate is the quantity of material removed since the end of its activity. Since our reconstructions take into account both dense and pyroclastic materials, our results are expressed as bulk erupted volumes instead of dense rock equivalent (DRE) volumes. It is important to mention that a significant part of the erupted magma might not have remained on the volcano itself (loose material either eroded soon after deposition, dispersed over wide areas as tephra fallouts, or displaced during sector collapse). Estimates of the emitted volumes and eruptive rates must therefore be considered as minimum values. Eruptive and erosion rates can also be biased by our non-exhaustive sampling, which may not cover the entire period of activity of the volcano. Finally, note that sector collapses, which are extremely short-lived processes that trigger debris avalanches and large volume transfer from the flank to the foot of the volcano, have not been considered for erosion rate calculations. In order to compare the surface erosion affecting the flanks of the Ecuadorian volcanoes, we have only considered the flanks non-affected by a sector collapse to calculate both eroded volumes and erosion rates. The total constructed (*Vc*) or eroded (*Ve*) volume corresponds to the integration of the elevation difference between the upper and the lower surface (Δz), over the area of the edifice. The volume uncertainty is defined as $\sigma_V = V.\frac{\sigma_z}{\Delta z}$, where the uncertainty of the elevation (σ_z) is $\sigma_z = \sqrt{{\sigma_{i\ surf}}^2 + {\sigma_{f\ surf}}^2}$, with $\sigma_{i\ surf}$ and $\sigma_{f\ surf}$ the uncertainty of the initial and final surface elevation, respectively. The latter is estimated to 200 m, based on the standard deviation of the elevation dispersion of the points selected around the surface model, and on the error map of the kriging interpolation method generated by the ArcGIS software (Germa et al. 2015; Ricci et al. 2015a). The volume is then divided by the activity or quiescence period of the volcano (ΔT_a and ΔT_q, respectively) to calculate their apparent magmatic output (*OR*) and erosion (*ER*) rates, with $OR = \frac{Vc}{\Delta T_a}$ and $ER = \frac{Ve}{\Delta T_q}$. The rate uncertainty is defined as $\sigma_R = R.\sqrt{\left(\frac{\sigma_V}{V}\right)^2 + \left(\frac{\sigma_T}{\Delta T}\right)^2}$ where *R* is the rate, *V* the volume, and σ_T the uncertainty of the duration of the activity or quiescence period, calculated from K-Ar ages uncertainties.

Results

K-Ar dating

Twenty new K-Ar ages are presented in Table 1 and Figs. 2 and 3. The average K content is 0.8, 1.5, and 2.0 wt.%, for the

separated plagioclase crystals, groundmass, and glass shards fractions, respectively. The highest radiogenic Ar content is 22.4% for sample 17EQ65, a lava flow from Cushnirumi volcano (Table 1).

The oldest age of 1038 ± 87 ka obtained from the *Mojanda-Fuya Fuya-Cushnirumi* complex is for the termination of a lava flow south of the complex (sample 17EQ61; Fig. 2a, b) and could correspond to a "pre-Mojanda" activity. We obtain 260 ± 4 and 194 ± 6 ka (17EQ68 and 17EQ62, respectively) for samples from the upper part of Lower Mojanda. These ages are younger than those obtained for Lower Fuya Fuya (476 ± 38 and 347 ± 7 ka, G-0001 and 17EQ71, respectively; Fig. 2a, b) and for the San Bartolo unit (316 ± 7 and 298 ± 8 ka, 17EQ72 and 17EQ70, respectively; Fig. 2b). The terminal domes of Upper Fuya Fuya are significantly younger, since the construction of the Colangal dome occurred at 28 ± 5 ka (17EQ64). Finally, despite a greater apparent erosion, we obtain 383 ± 6 and 411 ± 8 ka (17EQ65 and 17EQ67, respectively; Fig. 2a, b) for Cushnirumi lava flows, considering that, based on the crest morphology, the lava flow of sample 17EQ67 is related to Cushnirumi instead of Lower Fuya Fuya (Robin et al. 2009).

Regarding *Imbabura* volcano, we obtain an age of 21 ± 8 ka (sample 17EQ100) for the lava flow from the Angaraloma unit (Fig. 2c). We obtain 0 ± 27 ka (i.e., ≤ 27 ka taking into account the 1-σ uncertainty) for a lava flow from the eastern flank (17EQ82) that could also belong to the same eruptive stage, and 30 ± 3 ka for IMB71, a lava flow from the western flank of Taita Imbabura. Finally, as the juvenile block from the Huarmi Imbabura blast deposit is almost entirely crystallized (17EQ73; ESM 1), we failed at isolating enough quantity of groundmass. We thus performed analyses on plagioclase crystals and obtain an age of 15 ± 7 ka (17EQ73; Fig. 2c).

The new ages obtained for *Cubilche* lava flows provide new temporal constraints for its sector collapse. Indeed, we obtain 40 ± 5 ka for the older, pre-collapse edifice, and 45 ± 5 ka for the summit of the recent cone (Fig. 2c), constructed inside the collapse amphitheater. Taking into account 1-σ uncertainties, the collapse event is thus constrained between 40 and 45 ka. The amphitheater was then rapidly filled by the recent cone products. These results also show that Cubilche activity occurred during the main construction stage of Taita Imbabura, before the LGM period.

For the lava flows sampled from three different flanks and the summit area of *Cusín* volcano, we obtain four results in a remarkably narrow age range, from 495 ± 12 to 517 ± 8 ka (Fig. 2d). This edifice was therefore constructed in a relatively short period of time. Since its summit has the same age as the flanks and no debris avalanche deposit from Cusín have been documented in the Interandean Valley, the semi-circular depression seems to be rather related to erosion processes than sector collapse.

Whole-rock geochemical analyses

Results of major and trace element content analyses are available in ESM 2. Most samples plot in the andesite field in the K_2O vs. SiO_2 diagram (Fig. 4a), with some basaltic andesite and dacite rocks, and one rhyolite composition. The K_2O content ranges between 0.9 and 2.7 wt.%, for the summit lavas of Mojanda and Cusín volcanoes (17EQ63 and 17EQ98, respectively), and the silica content extends from 53.6 to 74.5 wt.%,

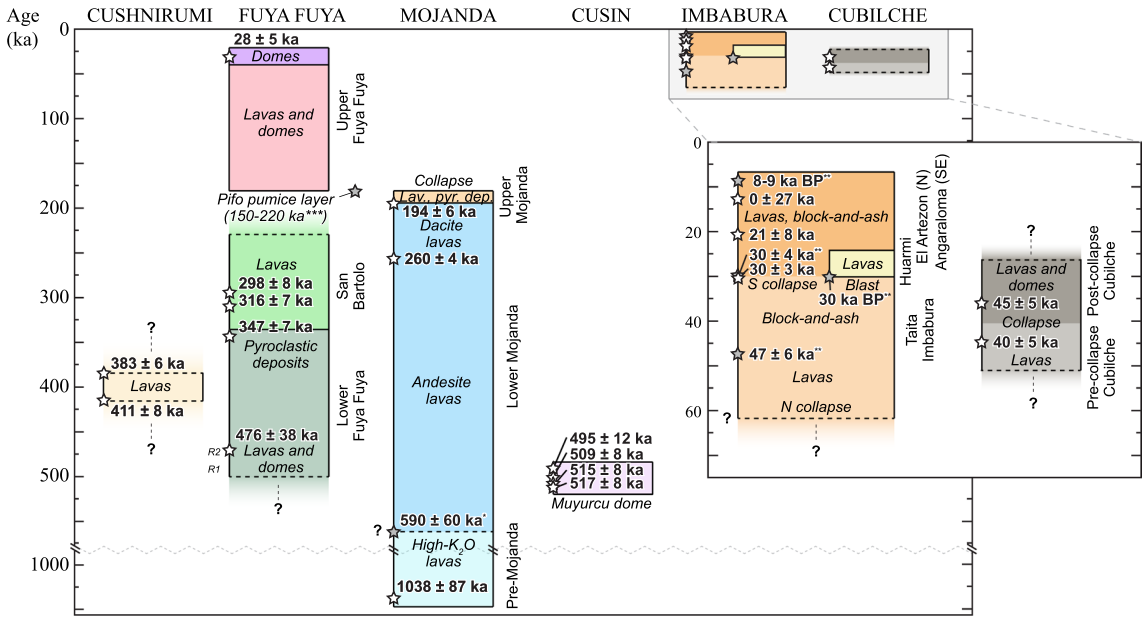

Fig. 3 Summarized stratigraphy of Cushnirumi, Fuya Fuya, Mojanda, Imbabura, Cubilche, and Cusín volcanoes. Same colors as Fig. 2. White stars: ages obtained in this study (Table 1). Gray stars: * whole-rock K-Ar age obtained by Barberi et al. (1988), ** ^{14}C and $^{40}Ar/^{39}Ar$ ages obtained by Le Pennec et al. (2011), *** Bigazzi et al. (1992); Hall and Mothes (1997). Lav. pyr. dep: lavas and pyroclastic deposits

for the summit of Mojanda (17EQ63) and the G-0001 pumice sample from Fuya Fuya, respectively. Our samples mainly belong to the medium-K calc-alkaline series (Fig. 4a). They display significant enrichment in Large-Ion Lithophile Elements (LILE; Rb, Ba, and K) and Light Rare-Earth Elements (LREE) relative to Heavy Rare-Earth Elements (HREE; Dy, Er, Yb; Fig. 4b, c), as well as depletion in Nb, Ti, and occasionally Eu, typical of arc magmas. However, the summit lava flow of Cusín (17EQ98) and the oldest lava flow of "pre-Mojanda" (17EQ61) are enriched in alkali elements and belong to the high-K calc-alkaline series (Fig. 4a).

Lava flows and pumice samples from *Mojanda* and *Fuya Fuya* plot in the fields defined by Robin et al. (2009), except the summit of Mojanda (17EQ63), which is a slightly less differentiated, and the ~ 1 Ma "pre-Mojanda" lava flow (17EQ61; Fig. 4a), whose data fall away from the whole Mojanda trend, supporting the fact that this lava flow belongs to an early Mojanda system. Furthermore, it can be noted that, compared to others, this sample is significantly enriched in most incompatible and Rare Earth elements (Fig. 4a, b). Samples 17EQ62, 17EQ68 and 17EQ69 clearly belong to the Mojanda series, although sample 17EQ69 is enriched in most incompatible and Rare Earth elements (Fig. 4b, c). The G-0001 pumice fallout is a rhyolite that plots in the Fuya Fuya composition field. Noticeably, the geochemical compositions of the three samples from *Cushnirumi* volcano are rather similar to Fuya Fuya samples for both major (Fig. 4a) and trace (Fig. 4b, c) element concentrations.

The composition of samples from *Imbabura* and *Cubilche* volcanoes is rather similar, with a homogeneous K_2O content of about 1 wt.% (Fig. 4a). All samples plot in the field previously obtained by Bryant et al. (2006), Andrade (2009), Andrade et al. (2019), and Le Pennec et al. (2011). They show no clear compositional change

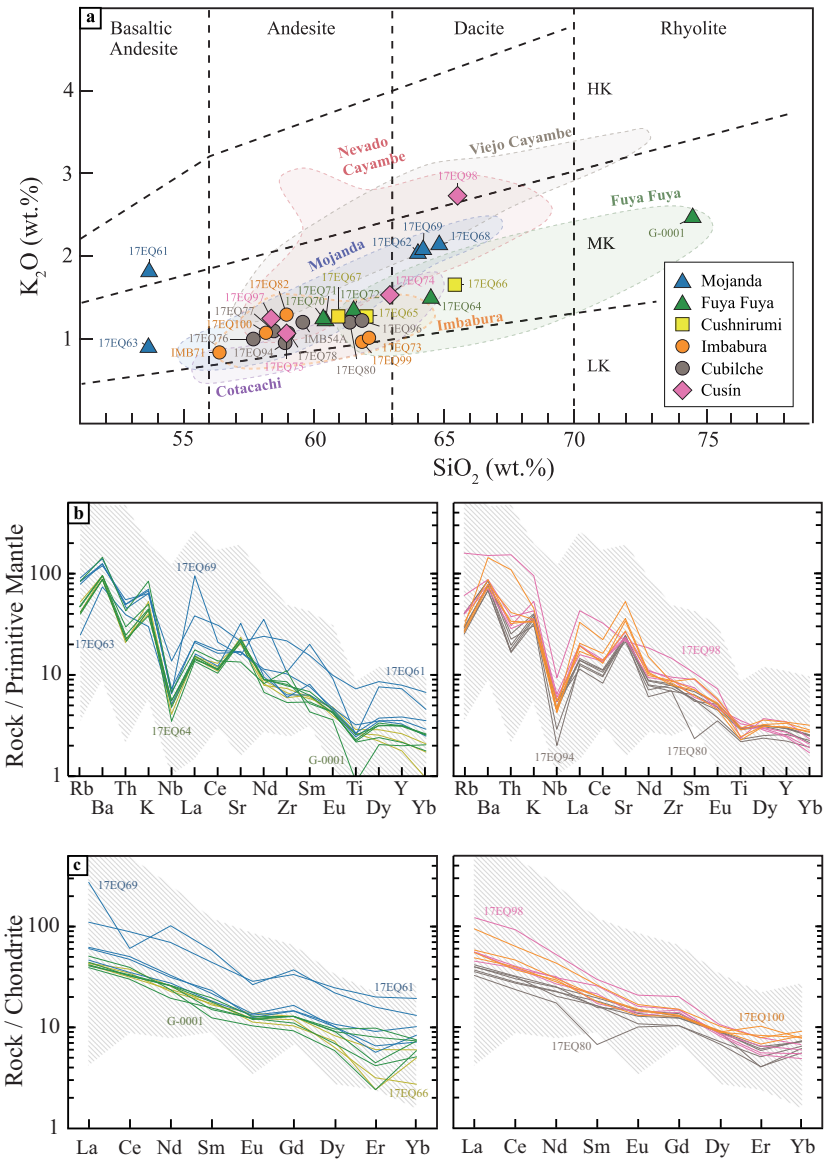

Fig. 4 **a** K_2O vs. SiO_2 diagram (Peccerillo and Taylor 1976) for samples from this study. Symbols are the same as used in Fig. 2. Colored composition fields show the range of values previously obtained for Mojanda (blue; Robin et al. 2009), Fuya Fuya (green; Robin et al. 2009), Imbabura (orange; Bryant et al. 2006; Le Pennec et al. 2011; Andrade et al. 2019), as well as Cayambe (red; Samaniego et al. 2005) and Cotacachi (purple; Almeida 2016), located east and west of our study area, respectively (Fig. 1). HK: high-K, MK: medium-K, LK: low-K calc-alkaline series. **b**, **c** Spider diagrams of incompatible and Rare Earth elements normalized to primitive mantle and chondrites, respectively (S-s and WF 1989). Left diagrams: spectra obtained for Cushnirumi (yellow), Fuya Fuya (green), and Mojanda (blue) samples. Right diagrams: spectra obtained for Cusín (pink), Imbabura (orange), and Cubilche (brown) samples (same colors as Fig. 4a). Hatched gray composition field represents the published dataset obtained across the whole Ecuadorian arc (whole-rock data from the Georoc database; http://georoc.mpch-mainz.gwdg.de/georoc/)

between older and younger samples, nor between pre and post-collapse events. Lava flows from Cubilche are slightly poorer in incompatible elements than those of Imbabura (Fig. 4b, c), with higher depletion in Nb for the summit sample (17EQ94), and in Sm for the distal southeastern lava flow (17EQ80; Fig. 2a). Similar compositional and geochronological signatures suggest that both edifices should belong to the same magmatic system.

Finally, despite close ages (Table 1), lava flows from *Cusín* volcano have a rather heterogeneous composition. Compared to andesite lava flows from the flanks, the summit dacite sample (17EQ98) is enriched in the most incompatible and Rare Earth elements (Fig. 4b, c).

Volumes, eruptive and erosion rate results

Volumes, eruptive and erosion rates calculated for the studied volcanoes are summarized in Table 2. Estimated volumes of erupted magmas range between 13 ± 6 and 132 ± 48 km^3, for Cubilche and Mojanda volcanoes, respectively, and the eroded volumes between 1 ± 1 and 47 ± 12 km^3, for Cubilche and Cushnirumi, respectively (Table 2). The eruptive rates vary significantly between ~ 0.2 and > 3.6 ± 2.1 km^3/kyr, for Mojanda and Imbabura volcanoes, respectively. Eruptive rates for Cushnirumi, Fuya Fuya and Imbabura are given as minimum values since we do not accurately know the extent of their period of activity (Fig. 3). The eruptive rate of Mojanda volcano has been calculated considering that its activity started at least at ~ 1.04 Ma (Fig. 3), and we have included age data obtained by Samaniego et al. (2005) and Le Pennec et al. (2011) to calculate Cayambe and Imbabura eruptive rates, respectively. Finally, the erosion rates range between 0.02 ± 0.01 (Cusín) and 0.14 ± 0.09 km^3/kyr (Mojanda; Table 2). We present Cushnirumi and Cubilche erosion rates as approximate values since their respective activity may have continued after the youngest age we obtained for these volcanoes (Fig. 3), and their quiescence period could therefore be slightly overestimated.

Discussion

Comparison between new and previous ages

Our new ages are in good agreement with the published data from Mojanda, Fuya Fuya, and Imbabura volcanoes (Robin et al. 2009; Le Pennec et al. 2011; Andrade et al. 2019).

The only available age for *Mojanda-Fuya Fuya-Cushnirumi* complex is a whole-rock K-Ar age of 590 ± 60 ka obtained for a lava flow of Mojanda (Barberi et al. 1988), for which neither the location nor the geological unit are mentioned. The oldest age that we obtained for this complex is 476 ± 38 ka (G-0001 from Fuya Fuya; Table 1; Fig. 3). Although the reliability of whole-rock K-Ar ages have been questioned (e.g., Samper et al. 2007; Bablon et al. 2018, 2019), if we assume that the age of 590 ± 60 ka is not biased by any argon contamination or potassium loss inherent to whole-rock measurements, we infer this age may correspond to the activity of Lower Mojanda, as suggested by Robin et al. (2009). Our new ages indicate that the San Bartolo sector collapse occurred after 194 ± 6 ka (17EQ62; Table 1), at the end of Upper Mojanda activity (Robin et al. 2009). As debris avalanche deposits are covered by the Pifo ash-fall layer (Robin et al. 2009), the youngest limit for this collapse is ~ 150–200 ka based on fission track age constraints (Bigazzi et al. 1992; Hall and Mothes 1997).

Our results obtained for *Imbabura* lava flows (30 ± 3, 0 ± 27 ka, and 21 ± 8, for the southwestern flank, southeastern flank, and the Angaraloma unit, respectively; Table 1; Fig. 2c) are in agreement with ^{40}Ar/^{39}Ar and ^{14}C ages obtained by Le Pennec et al. (2011). Barberi et al. (1988) obtained a whole-rock K-Ar age of 1.76 ± 0.18 Ma for an andesite lava flow attributed to Imbabura. As the sampling location is not specified, their sample could either have been collected in the basement, or the result is erroneous due to whole-rock concerns. This age therefore will not be further considered. Finally, we obtained an age of 15 ± 7 ka (Table 1) for the plagioclase phenocrysts separated from a juvenile block from

Table 2 Results of volumes, eruptive and erosion rates calculations obtained from the numerical paleosurfaces and given at 1-sigma accuracy. Rate obtained of < 35 ka products of Imbabura volcano are from Le Pennec et al. (2011). A: andesite, D: dacite, R: rhyolite

Volcano	Stage	Magma type	Construction				Erosion			
			Volume (km^3)	Period (ka)	Duration (kyr)	Eruptive rate (km^3 kyr^{-1})	Volume (km^3)	Period (ka)	Duration (kyr)	Erosion rate (km^3 kyr^{-1})
Cayambe	Viejo	A-D-R	115 ± 5	~ 1108–1050	~ 58 ± 12	~ 1.5	25 ± 14	1050–0	1050 ± 5	0.02 ± 0.01
	Nevado	A-D-R	150 ± 20	409–0	409 ± 4	~ 0.39				
Cubilche	Whole	A	13 ± 6	45–~ 40	~ 5 ± 7	2.6 ± 3.9	1 ± 1	~ 40–0	~ 40 ± 5	~ 0.02 ± 0.02
Cushnirumi	Whole	A	53 ± 25	> 411–~ 383	> 28 ± 10	> 1.9 ± 1.1	47 ± 12	~ 383–0	~ 383 ± 6	~ 0.12 ± 0.03
Cusín	Whole	A	43 ± 17	517–495	22 ± 14	2.0 ± 1.5	8 ± 5	495–0	495 ± 12	0.02 ± 0.01
Fuya Fuya	Lower FF.	A-D	31 ± 19	> 476–347	> 129 ± 39	> 0.2 ± 0.2				
Imbabura	Pre-Huarmi	A-D	61 ± 24	> 47–30	> 17 ± 7	> 3.6 ± 2.1				
	Post-Huarmi	A-D	> 4.6	35–0	35	> 0.13	4 ± 4	30–0	30 ± 4	0.1 ± 0.2
Mojanda	Whole	A	132 ± 48	~ 1038–194	~ 844 ± 87	~ 0.2 ± 0.1	27 ± 18	194–0	194 ± 6	0.14 ± 0.09

Huarmi blast deposits (17EQ73), previously dated by ^{14}C on two charcoal samples at 29.2–30.5 and 31.1–31.5 ka cal BP (Le Pennec et al. 2011). Ages agree only at the 2-σ level, but our K-Ar result should be considered with caution since the measurement conditions were not ideal, due to the lack of groundmass of this sample, the low potassium content of plagioclase crystals analyzed, and the resulting low radiogenic argon content (0.8 and 0.2%, respectively; Table 1).

Eruptive history of the northern segment

Figure 5 shows the evolution of the Ecuadorian arc morphology within our study area during the late Quaternary.

Before ~ 1.2 Ma, the landscape was shaped by the basement constituting the two Cordilleras and the Interandean Valley in between (Fig. 5a). Only the Chacana volcanic complex, located south of our study area (Fig. 1), was active since at least ~ 2.6 Ma (Opdyke et al. 2006). Thick sequences of volcanoclastic deposits, the Angochagua formation, which covers the Eastern Cordillera, as well as Pisque and San Miguel formations in the Interandean Valley, could have been emplaced between the Late Miocene and the Early Pleistocene (e.g., Boland et al. 2000; Andrade 2009; Alvarado et al. 2014). The construction of the current arc seems to have started at about 1.1–1.0 Ma (Table 1; Samaniego et al. 2005) with the coeval activity of Viejo Cayambe in the Eastern Cordillera (red; Fig. 5b) and the "pre-Mojanda" edifice in the Interandean Valley (turquoise; Fig. 5b). Following an apparently long period of quiescence and erosion, volcanic activity resumed with the rapid construction of Cusín volcano (pink; Fig. 5c) between 550 and 450 ka, in the eastern side of the Interandean valley. The onset of Lower Mojanda construction could have occurred during this period. Then, the rather coeval construction of the main edifices of Lower and Upper Mojanda (blue), Fuya Fuya (green) and Cushnirumi (yellow; Fig. 5d) occurred, since at

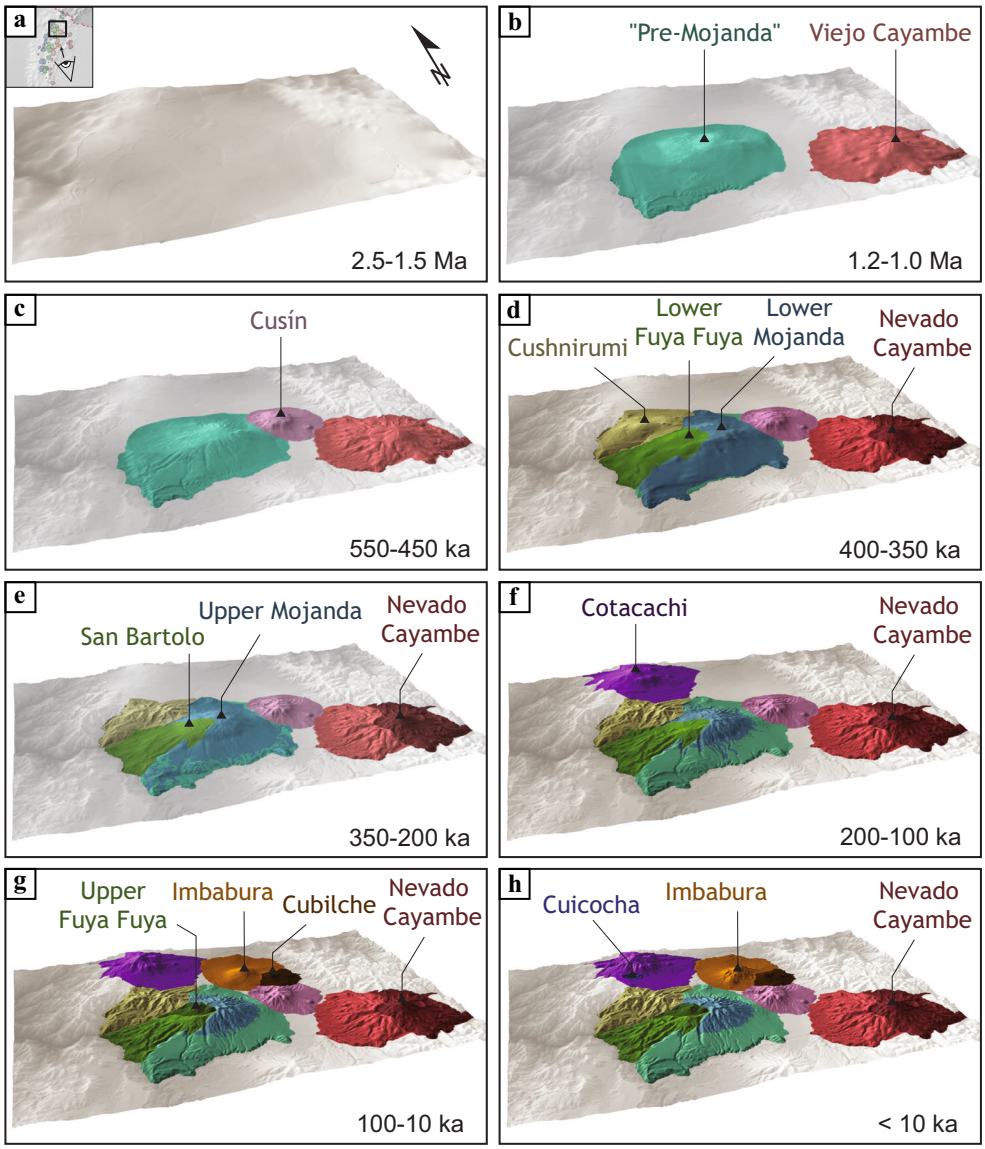

Fig. 5 Synthesis cartoons of the paleotopography evolution of the E-W segment located between Cotacachi and Cayambe volcanoes, north of the Ecuadorian arc (Fig. 1), between 2.5 and 1.5 Ma (**a**), 1.2 and 1 Ma (**b**), 550 and 450 ka (**c**), 400 and 350 ka (**d**) 350 and 200 ka (**e**), 200 and 100 ka (**f**), 100-10 ka (**g**), and for the past 10 ka (**h**) . Note that both landscape morphology before the construction of volcanoes and evolution of their erosion are speculative, and subjectively deduced from present elevations

least 476 ka for Fuya Fuya and 411 ka for Cushnirumi volcano (Table 1). The period of activity of Cushnirumi may have been short and ended about 383 ka (Table 1). In the Eastern Cordillera, Nevado Cayambe (dark red; Fig. 5d) started its growth with the so-called Angureal edifice (450 ka), followed by the construction of the Nevado Cayambe main summit (< 250 ka; Samaniego et al. 2005). Constructions of both San Bartolo cone (~ 350–290 ka) and Upper Mojanda (~ 250–190 ka; Table 1) followed Cushnirumi activity (Fig. 5e) and experienced a major westwards sector collapse at about 160 ka (Robin et al. 2009).

Between 195 and 100 ka, the volcanic activity seems to have migrated north-westward with the construction of Upper Fuya Fuya within the Mojanda and Lower Fuya Fuya collapse amphitheater (Robin et al. 2009), and Cotacachi volcano in the Western Cordillera (purple; Fig. 5f; Almeida 2016; Bablon 2018). The western and eastern flanks of this latter volcano could have also collapsed during this period, covering a part of the Interandean Valley north of Mojanda volcano. In the Eastern Cordillera, Nevado Cayambe was still active (Samaniego et al. 2005).

In the Interandean Valley, onset of Imbabura (orange; Fig. 5g) and Cubilche (brown) activities have occurred at least since 47 ± 6 ka (Le Pennec et al. 2011) and 40 ± 5 ka (Table 1), respectively. However, few ages are available for Taita Imbabura, and its construction period is still poorly constrained. The northern flank of Imbabura volcano experienced at least one sector collapse, whose scars have been progressively erased by subsequently emitted material that filled the amphitheaters. The northern flank of Cubilche also collapsed most likely between 40 and 45 ka (Table 1), and the resulting amphitheater was partly filled by a new cone. The summit domes of Upper Fuya Fuya (dark green; Fig. 5g) grew shortly before the Last Glacial Maximum (28 ± 5 ka; Table 1), as well as the Huarmi Imbabura dome complex (~ 30 ka; Le Pennec et al. 2011), followed by both El Artezon cone in the north and Angaraloma unit on the southeastern flank. In the Eastern Cordillera, the Nevado Cayambe main summit was still active. Lastly, during the Holocene (< 10 ka), pyroclastic flow deposits were emplaced east of Imbabura about 9 ka (Le Pennec et al. 2011), and the Cuicocha caldera-forming eruption took place at 3 ka on the southern foot of Cotacachi volcano (dark green; Fig. 5h; Hillebrandt 1989). Nevado Cayambe is presently the most active edifice of this area, and its eastern summit, not affected by Holocene glaciations, has been constructed during the last 4 kyr (Samaniego et al. 1998).

Eruptive rates

Eruptive rates obtained at the Ecuadorian arc scale, including those calculated following the present approach for Mulmul, Huisla and Igualata volcanoes from the southern termination of the arc (Bablon et al. 2019), are shown in Fig. 6a. As

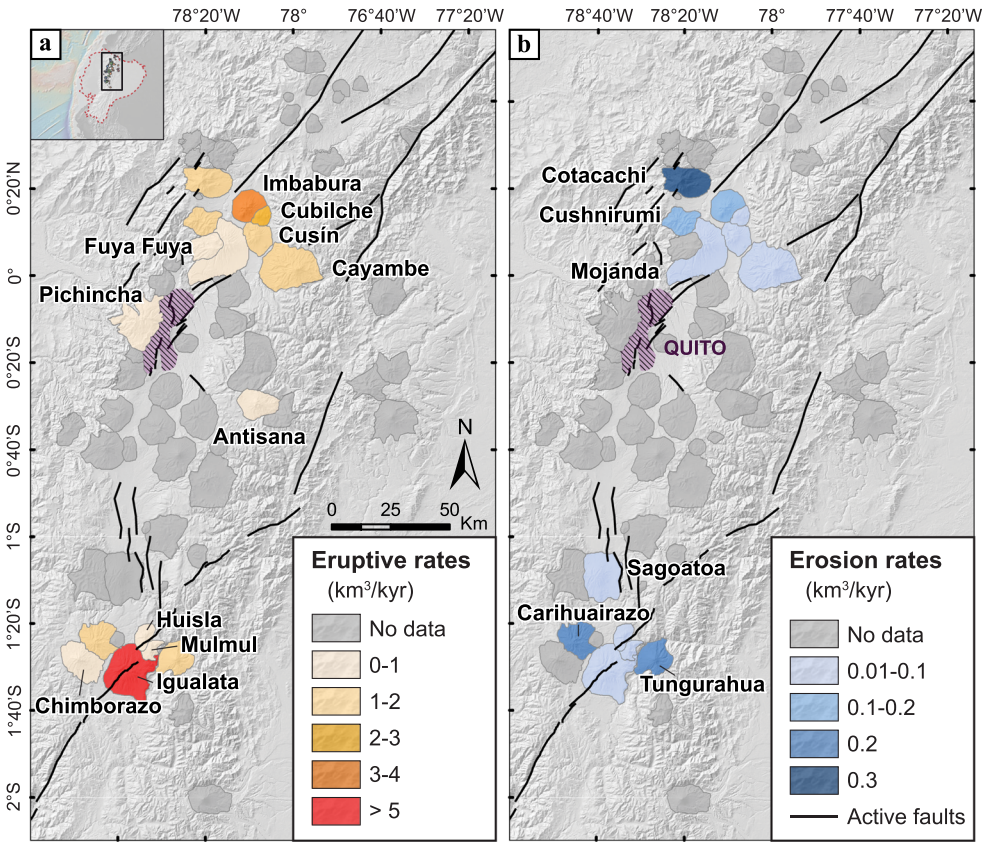

Fig. 6 Summary maps of eruptive (**a**) and erosion (**b**) rates presented in this study, as well as those previously calculated for Cayambe (Samaniego et al. 2005), Imbabura (Le Pennec et al. 2011), Pichincha (Robin et al. 2010), Chimborazo (Samaniego et al. 2012), Cotopaxi (Hall and Mothes 2008), Tungurahua (Bablon et al. 2018), Carihuairazo and Cotacachi (Bablon 2018). Detail of these rates is available in Table 3. Black lines represent the main crustal active faults (modified from Egüez et al. 2003; Alvarado et al. 2014, 2016; Almeida 2016; Baize et al. 2016). Note that activity periods are constrained by a variable number of ages, about twenty for Tungurahua and Pichincha, and less than five for Cushnirumi, Imbabura, and Igualata volcanoes, for instance

mentioned before, eruptive rates could be biased by sector collapses, as well as the dispersed pyroclastic material, the volume of which could be much higher than that of lava flows emitted (Erlund et al. 2010). As it depends on eruptive dynamics, it is therefore not possible to determine the proportion of pyroclastic material involved, and each eruptive rate must be considered as a minimum. Incomplete sampling could also lead to erroneous determination of eruptive and erosion rates. For instance, as it is possible that oldest ages obtained for Cushnirumi, Lower Fuya Fuya and Imbabura do not correspond to the beginning of their construction (Fig. 3), leading to overestimation of their eruptive rate. At a first glance, there are no significant difference between rates from the northern part of the arc and its southern termination, as well as no strong correlation between the eruptive rates and the proximity of the active crustal faults (Fig. 6a), whose identification and mapping require refinements. Note that eruptive rates obtained for both Igualata and Mojanda volcanoes could be overestimated as the onset of their activity is not well constrained (Bablon et al. 2019; Table 1).

We show in Fig. 7a the eruptive rates obtained in this study (colored circles), as a function of the activity duration used to calculate these rates. The figure highlights that eruptive rates can significantly vary over intervals shorter than 100 kyr, ranging between 0 and 6 km^3/kyr, whereas they are systematically lower than 1 km^3/kyr for intervals larger than 100 kyr. Figure 7a shows that eruptive rates obtained for other worldwide Quaternary arc volcanoes (Table 3) display a trend similar to that of Ecuadorian volcanoes. Our results therefore strongly support the hypothesis that emission rates are characterized by sporadic activity phases separated by quiescence periods of variable duration (Hildreth and Lanphere 1994; Lewis-Kenedi et al. 2005; Bacon and Lanphere 2006; Samaniego et al. 2016; Bablon et al. 2018; Grosse et al. 2018). In other words, many andesitic volcanoes are constructed by activity spurts with variable and relatively high emission rates over time periods usually shorter than 100 kyr (Fig. 7a), whereas longer time periods systematically include long quiescence periods that lower the averaged apparent eruptive rate. Note that eruptive rates reported for Ecuadorian volcanoes by Martin et al. (2014; between 0.13 and 2.2 km^3/kyr) are higher than those obtained in Chile, Mexico and in the Cascades range (between 0.05 and 0.2 km^3/kyr). However, this can be explained by the short activity period of ~ 2 to 35 kyr used for Ecuadorian volcanoes while eruptive rates for other volcanoes are much larger (~ 0.1 to 1 Myr) and probably include quiescence periods that reduce the averaged apparent eruptive rates (Fig. 7a).

Eruptive rates are controlled by magma production rates. However, we note that the trend of eruptive rates (Fig. 7a) is similar for both fast (~ 6–10 cm $year^{-1}$; e.g., Andes, Cascade arc, Alaska, Japan) and slow (~ 2 cm $year^{-1}$; Lesser Antilles)

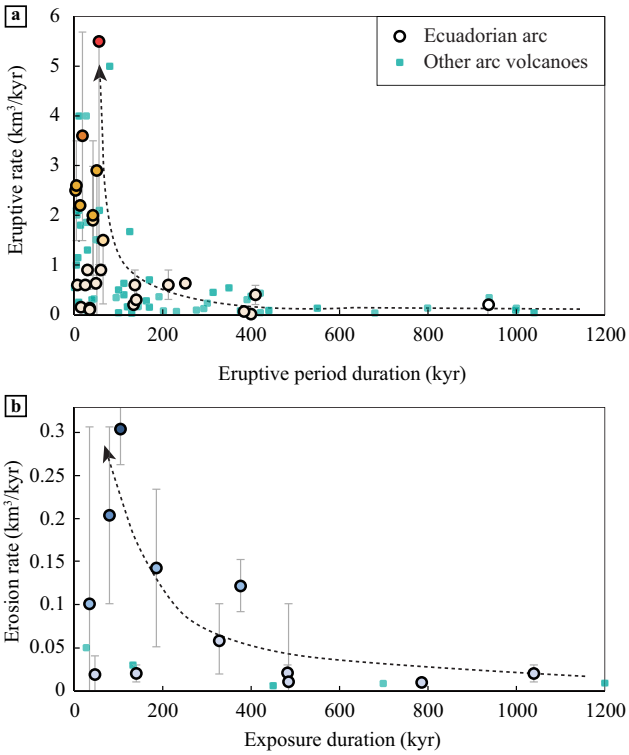

Fig. 7 **a** Eruptive rates as a function of the timespan used to calculate the rates. Results obtained for Ecuadorian volcanoes are represented by circles with bold outlines. Colors are the same as used in Fig. 6a. Previously published data obtained for other volcanoes associated with subduction are represented by turquoise squares (Crisp 1984; Hildreth and Lanphere 1994; Feeley and Davidson 1994; Thouret et al. 2001; Harford et al. 2002; Hildreth et al. 2003a, 2003b; Le Friant et al. 2004; Ownby et al. 2007; Frey et al. 2004; Lewis-Kenedi et al. 2005; Bacon and Lanphere 2006; Hora et al. 2007; Singer et al. 2008; Klemetti and Grunder 2008; Germa et al. 2010; Karátson et al. 2012; Lahitte et al. 2012; Ricci et al. 2015a, 2015b; Germa et al. 2015; Samaniego et al. 2016; Grosse et al. 2018). **b** Erosion rates as a function of the exposure duration of rock, i.e., the end of the volcanoes activity. Published data obtained for other arcs are represented by turquoise squares (Ricci et al. 2015a, 2015b; Germa et al. 2015). Colors are the same as used in Fig. 6b. Details of the volcanoes considered, periods, and volumes are given in Tables 2 and 3

convergence subduction zones. Consequently, eruptive rates do not seem to be directly linked to the convergence velocity of the subducting plate. Output rates are also controlled by the magma viscosity and volatile content (White et al. 2006; Zellmer et al. 2015) and the crust thickness (Hawkesworth et al. 2004), whereas magma rise could be favored by sector collapses (Presley et al. 1997), ice retreat at the end of glacial periods (Bacon and Lanphere 2006), mafic magma recharge in the chamber (Rampino et al. 1979), or large earthquakes. Eruptive rates could therefore be controlled by several factors, which could explain the large difference in rates observed for time periods shorter than 100 ka (Fig. 7a), but the time interval considered for eruptive rate calculations appears as a key parameter.

Table 3 Results of eruptive and erosion rates obtained for other volcanoes, from subduction or hot-spot contexts

Volcano	Stage	Age max.	Age min.	Duration	Volume total	Eruptive rate		Erosion rate			Reference
		ka	ka	kyr	km^3	km^3/kyr	mm/yr	km^3/kyr	mm/yr	T/km^2/kyr	
Tungurahua	I	293 ± 10	81 ± 3	212 ± 10	124 ± 74	0.6 ± 0.3	3.6 ± 2.2				Bablon et al. (2018)
	I	81 ± 3	0	81 ± 3	16 ± 4			0.2 ± 0.1	2.4 ± 0.6	6.5 ± 1.7	
	II	29 ± 2	2.96 ± 0.03	26 ± 2	24 ± 4	0.8 ± 0.2	17.8 ± 3.4				Bablon et al. (2018), from Hall et al. (1999)
	III	2.96 ± 0.03	0	2.96 ± 0.03	7 ± 3	2.5 ± 1	41.5 ± 17				Bablon et al. (2018), from Hall et al. (1999)
	Whole	293 ± 10	0	293 ± 10	108 ± 30	0.4 ± 0.1	2.4 ± 0.7				
Mulmul	Whole	174 ± 3	145 ± 4	39 ± 12	22 ± 7	0.6 ± 0.3					From Bablon et al. (2019)
		145 ± 4	0	145 ± 4	7 ± 2			0.02 ± 0.01			
Igualata	Main edifice	> 376 ± 10	337 ± 7	> 39 ± 12	217 ± 45	< 5.6					From Bablon et al. (2019)
		337 ± 7	0	337 ± 7	19 ± 14			0.06 ± 0.04			
Huisla	Whole	612 ± 10	492 ± 9	120 ± 13	25 ± 11	0.2 ± 0.1					From Bablon et al. (2019)
		492 ± 9	0	488	2 ± 2			0.01 ± 0.01			
Sagoatoa	Whole	799 ± 12	0	799 ± 12	8 ± 3			0.01 ± 0.00			From Bablon et al. (2019)
Antisana	I	> 400		> 400	~ 5.4	< 0.01					From Hall et al. (2017)
	II	> 400	15	> 385	~ 33	< 0.09					
	III	> 15		15	~ 2.2	~ 0.15					
Pichincha	Lower Rucu	850	600	250	~ 160	~ 0.64					Robin et al. (2010)
	Basal Guagua	60	47	13	~ 29	~ 2.2					
	Main Guagua	60	11	49	32 ± 1	~ 0.63					
	Toaza	11	4	7	4 ± 1	0.6 ± 0.1					
Cayambe	Viejo	~ 1110	1045	> 65	115 ± 5	< 1.5					From Samaniego et al. (2005)
		1045	0	1045	25 ± 14			0.02 ± 0.01			
	Nevado	409	0	409	150 ± 20	~ 0.39					
Chimborazo	I	120	60	60	52 ± 7	0.9 ± 0.1					Samaniego et al. (2012)
	II	60	35	25	14 ± 4	0.6 ± 0.1					
	III	35	0	35	4 ± 1	~ 0.1					
Parinacota (Chile)	Whole	163	0	163	46 ± 5	0.28 ± 0.03					Hora et al. (2007)
	Young cone	~ 5	0	~ 5	15 ± 4	0.99 ± 0.24					
Puyehue-Cordón Caulle (Chile)	Whole	314 ± 13	0	314 ± 13	131	> 0.42					Singer et al. (2008)
Aucanquilcha (Chile)	Azufrera	1040	920	120	21	0.16					Klemetti and Grunder (2008)
	Whole	1040	0	1040	38	0.04					
Ollagüe (Chile-Bolivia)	Whole			~ 130	3.6	~ 0.03	0.11				From Karátson et al. (2012)
	Whole			< 1000	~ 85	< 0.09					From Feeley and Davidson (1994)
Maricunga (Chile)	Whole			~ 14,600	23		0.007				
El Misti (Peru)	Whole	112	0	112	70–83	0.63					Thouret et al. (2001)
	Peak eruption rates			~ 10		2.1					
Payún Matrú (Argentina)	Whole	272 ± 5	261 ± 4	~ 11	~ 40	~ 4					Germa et al. (2010)
Ceboruco (Mexico)	Whole	~ 100	0	~ 100	51 ± 2.5	~ 0.51					From Frey et al. (2004)
Tancitaro (Mexico)	Whole			> 793 ± 22	> 97 ± 3	~ 0.12					From Ownby et al. (2007)
Tequila (Mexico)	Whole	~ 1000	0	~ 1000	106–149	~ 0.13	~ 0.79				From Lewis-Kenedi et al. (2005)
	Cerro Tomasillo	66 ± 20	58 ± 10	8 ± 22	1.9 ± 0.2	> 0.24					
Arenal (Costa Rica)	Whole			0.5	0.26	0.55					Crisp (1984)
Fuego (Guatemala)	Whole			57	50	2.1					Crisp (1984)
Ampato-Sabancaya	Whole A.	450	10	440	38–42	0.08–0.09					Samaniego et al. (2016)

Table 3 (continued)

Volcano	Stage	Age max.	Age min.	Duration	Volume total	Eruptive rate		Erosion rate			Reference
		ka	ka	kyr	km^3	km^3/kyr	mm/yr	km^3/kyr	mm/yr	T/km^2/kyr	
(Peru)	Basal S.	10–6	3	3–7	5–8.1	1.5–2.7					
	Whole S.	10–6	0	10–6	6–10	0.6–1.7					
Incahuasi (Argentina-Chile)	Whole	1570 ± 100	350 ± 30	1220 ± 130	62 ± 6	0.04–0.06					Grosse et al. (2018)
Falso Azufre	Quaternary pulse	910 ± 220	530 ± 90	380 ± 310	75 ± 13	0.1–1.3					
El Cóndor	Cóndor stage	130 ± 20	20 ± 30	110 ± 40	41 ± 15	0.2–0.7					
Mt. Fuji (Japan)	Whole			80	400	5					Crisp (1984)
Asama (Japan)	Whole			30	37	1.3					Crisp (1984)
Sakurajima (Japan)	Whole			14	25	1.8					Crisp (1984)
Hanoke (Japan)	Whole			400	150	0.37					Crisp (1984)
Mt. Baker (Cascades)	Whole	1290	990	300		0.17–0.27					Hildreth et al. (2003a)
		1180	990	190		0.27–0.43					
		900	500	400		0.02–0.04					
		280	50	230		0.03–0.07					
				~43	15 ± 3	~0.3					
Mt. Adams (Cascades)	Whole	940	0	940	~315 ± 84	0.25–0.4					Hildreth and Lanphere (1994)
		940	520	~420		0.015–0.04					
		400	125	~275		0.05–0.1					
		125	100	~25	12–24	0.5–1					
	Hellroaring cone			~25	75–125	3–5					
	Late Pleistocene cone			~25	39–52	1.6–2.1					
Mt. Mazama (Cascades)	Whole	420	0	420	176	0.42					Bacon and Lanphere (2006)
		420	30	390	112	0.29					
Katmai (Alaska)	Whole			100	70	0.5–1.2					Hildreth et al. (2003b)
	Mt. Griggs				35 ± 5	~0.0					
	Mt. Katmai				70 ± 18	~0.1					
		280	50	230		~0.2					
				~43	15 ± 3	~0.3					
Martinique Island	Mt Pelée	550	0	550	72.2	0.13					Germa et al. (2015)
		25	0	25	1.2 ± 0.5			0.05 ± 0.02	1.4 ± 0.2		
Montserrat Island	Soufrière Hills	170	0	170	~20	0.15					Harford et al. (2002)
		174	0	174		0.17					Le Friant et al. (2004)
	Silver Hills	1200	0	1200				0.0125			
Guadeloupe Island	Grande Découverte	250	150	100	4 ± 1	0.04 ± 0.01					Lahitte et al. (2012)
	Old Axial Chain	1000	650	350	189 ± 30	0.54 ± 0.09					
	Monts-Caraïbes	472	0	450	1 ± 1					0.23 ± 0.20	Ricci et al. (2015a)
	Beaugendre Valley	712 ± 12	0	700	8 ± 3					1.35 ± 0.55	
	MMC massif	681 ± 12	509 ± 10	170	4 ± 1	0.7					Ricci et al. (2015b)
	Sans-Toucher	451 ± 13	412 ± 8	40	10 ± 4	0.3 ± 0.1			0.3 ± 0.1	0.94 ± 0.38	
La Réunion Island	Cilaos and Mafate c.	180	0	180	> 214 ± 62			> 1.2 ± 0.4			Salvany et al. (2012)

Erosion rates

Comparison of erosion rates from different volcanic contexts

Considering that the youngest age obtained for each volcano (Table 1; Hall and Mothes 1997; Samaniego et al. 2005; Le Pennec et al. 2011) marks the end of its activity and consequently the beginning of an erosion period during which the volume of eroded material is significantly higher than the volume of material being emitted, erosion rates calculated in Ecuador vary between 0.010 ± 0.004 and 0.27 ± 0.04 km^3/kyr (Tables 2 and 3; Figs. 6b and 7b). There is no clear correlation between these rates and the presence of the main active faults (Fig. 6b), but a geographical relation can be inferred. Highest erosion rates are obtained for Cotacachi, Carihuairazo and Tungurahua volcanoes, located in both Western and Eastern Cordilleras (Fig. 1), whereas lowest rates are obtained for volcanoes located in the Interandean Valley (Fig. 6b), where the climate is drier and the surrounding relief gradients are smaller. Indeed, mean annual rainfall in the Eastern and Western Cordilleras vary between 1000 and 3000 mm/year, while they only reach 200–800 mm/year in the Interandean Valley (Clapperton 1990; www.inamhi.gob.ec). Moreover, the present-day equilibrium line altitude (ELA) of glaciers varies between 4150 and 5100 m a.s.l. for volcanoes from both Cordilleras, such as Chimborazo, Cayambe, Tungurahua, Antisana and Altar (Fig. 1; e.g., Clapperton 1990; Cadier et al. 2007; Cáceres 2010), and between 4400 and 5000 m for Cotopaxi volcano in the Interandean Valley. Moraine deposits indicate that the ELA could have reached 3500 m during the LGM for the eastern side of Chimborazo volcano (Clapperton 1990; Samaniego et al. 2012). Higher erosion rates associated to volcanoes located in the Cordilleras could therefore be related to orographic rainfall patterns and the presence of glaciers, the respective contribution of which cannot be accurately distinguished based on our data.

Although few data are available for other arc volcanoes, the erosion rates obtained in Ecuador are higher than those obtained in the Lesser Antilles (turquoise squares; Fig. 7b), despite similar annual rainfall regimes. Higher rates obtained in Ecuador can be related to the Quaternary glaciations and the strong abrasion that occurred during glacier retreats.

Erosion rates calculated in Ecuador are significantly lower than those obtained at La Réunion Island (> 1.2 km^3/kyr; Salvany et al. 2012). The high erosion rate of La Réunion Island could be due to significantly stronger rainfall, which varies there between 1000 and 12,000 mm/year. In addition, La Réunion Island is mainly made of basaltic lava flows (Salvany et al. 2012), whose erosion appears more efficient than for more evolved products from subduction zones (Bluth and Kump 1994; Louvat and Allègre 1997; Dupré et al. 2003; Vance et al. 2009).

Relationship between weathering and exposure duration

Several studies from various geological settings have described a power law relationship between volcanoes erosion rates and exposure duration (Taylor and Blum 1995; Kennedy et al. 1998; Gíslason et al. 1996; Karátson et al. 2012; Rad et al. 2013). Such trend is also suggested by our data for Ecuadorian volcanoes (Fig. 7b), with scattered values that reach 0.27 ± 0.04 km^3/kyr for volcanoes extinct since less than 400 ka, and low erosion rates not exceeding 0.05 km^3/kyr for longer exposure durations. Consequently, physicochemical erosion appears highest for rocks recently exposed at Earth's surface for some tens of thousands years, and significantly decreases for older rocks. The high weathering rate of younger volcanic products could be favored by the young unconsolidated cover and the lack of vegetation on the steep slopes of the volcanoes (Karátson et al. 2012). The decrease of the erosion rate with time could thus be related to the progressive removal of tephra and non-indurated material, the stabilization of a drainage network (Karátson et al. 2012), as well as rapid alteration of easily weathered material, recalling the effects of climate changes all along these periods and the progressive reaching of an equilibrium profile.

Influence of the Carnegie Ridge on the productivity rate and geochemistry of magmas

Major and trace elements obtained in our study area highlight a difference between both ~ 1 Ma old "pre-Mojanda" (17EQ61; Table 1) and Viejo Cayambe (Samaniego et al. 2005), and products younger than 600 ka. We notice, for example, a slight increase of Sr/Y and La/Yb ratios and a decrease of Y and Yb contents through time (Fig. 8b–d), for a rather homogeneous silica content (Fig. 8a). Such difference between old (≥ 1 Ma) and younger magmas have already been observed on the scale of single volcano for Atacazo (Hidalgo 2006), Iliniza (Hidalgo et al. 2007), and Pichincha (Robin et al. 2010; Samaniego et al. 2010) volcanoes (Fig. 1). The magma genesis processes that could explain such evolution are still debated (e.g., Samaniego et al. 2002; Bourdon et al. 2002; Robin et al. 2009; Chiaradia et al. 2009), but it seems to only affect volcanoes located in the northern part of the arc.

Although there is no correlation between output rates calculated for individual Ecuadorian Quaternary volcanoes (Table 2) and their spatial distribution, their number and basal surface significantly increase in the inland prolongation of the subducting Carnegie Ridge (Fig. 9a). Noticeably, the three largest volcanoes, Cayambe, Mojanda and Pichincha, are located near the Equator, in the midst of the inland prolongation of the Carnegie Ridge (Fig. 1). Hence, it can be inferred that the subduction of this ridge may have favored magma genesis at depth and could explain the increase in volcanic activity observed in northern Ecuador during the Late Quaternary

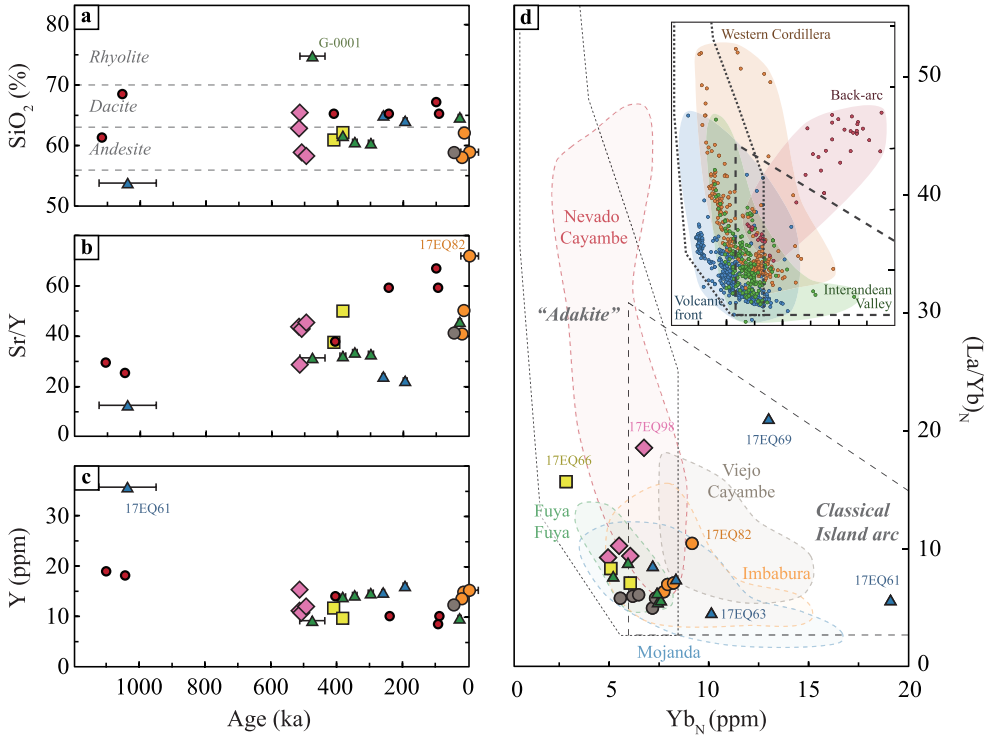

Fig. 8 **a**–**c** Variation of the silica content, Sr/Y ratio, and Y content in our dated samples, respectively, as a function of time. Legend of symbols is given in Fig. 3. Red circles: Cayambe volcano (Samaniego et al. 2005). **d** La/Yb ratio as a function of Yb content, normalized to chondrites (Sun and McDonough 1989). Classical Island arc and "adakite" composition fields are those proposed by Drummond and Defant (1990) and Martin (1999). Colored fields represent data obtained for Cayambe, Imbabura, Mojanda, and Fuya Fuya volcanoes (Samaniego et al. 2005; Bryant et al. 2006; Robin et al. 2009; Schiano et al. 2010; Le Pennec et al. 2011; Ancellin et al. 2017; Georgatou et al. 2018). Inset depicts the composition fields for all volcanoes of the arc (data from the Georoc database; http://georoc.mpch-mainz.gwdg.de/), located in the Western (blue) and Eastern (Orange) Cordilleras, Interandean Valley (green), and back-arc region (red)

(Fig. 9a; Martin et al. 2014). The along-arc variation of Y and Yb contents of lava flows from Ecuador and Colombia (Fig. 9b; Bourdon et al. 2004; Ancellin et al. 2017) also highlights that these contents are lower for volcanoes located above the eastern prolongation of the Carnegie Ridge. Nevertheless, more detailed studies about the influence of the Carnegie Ridge on productivity and geochemistry of magmas are needed to assess these preliminary inferences,

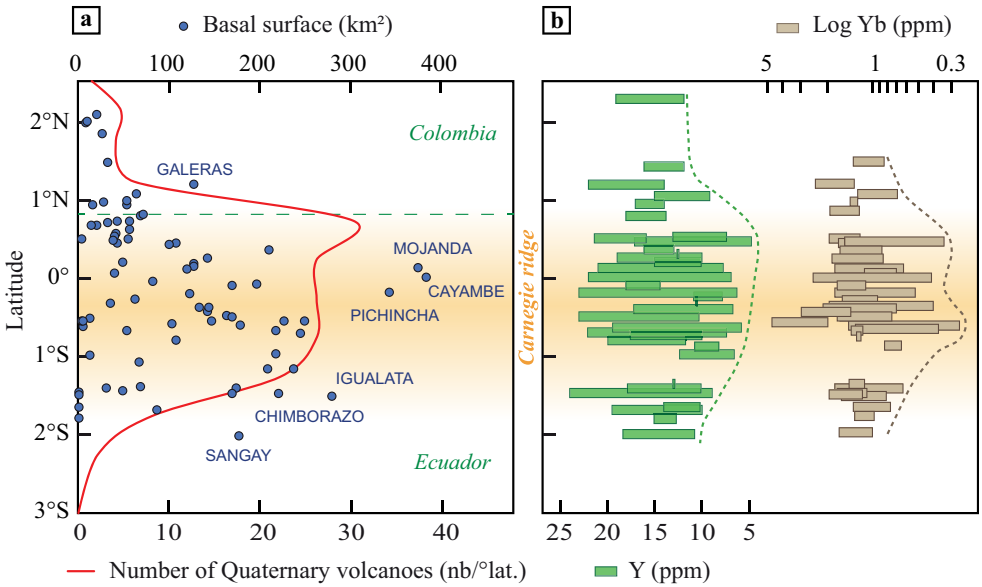

Fig. 9 **a** Basal surface of volcanoes (blue circles) and number of Quaternary volcanoes (red line) in the Northern Andes as a function of the latitude. Basal surfaces were calculated using the map of Bernard and Andrade (2011). The number of volcanoes was calculated for 0.5° latitude steps. The green dashed line represents the border between Ecuador and Columbia. **b** Variation of Y and Yb content as a function of the latitude (modified from Bourdon et al. 2004 and Ancellin et al. 2016, respectively). The location of the Carnegie Ridge is represented by the field in orange gradient, since its prolongation below the arc is oblique (Fig. 1)

and more geochronological constraints, volume and eruptive rate data are still required to further investigate the relationship between volcanic activity and geodynamics.

Conclusions

Our new K-Ar ages show that the volcanic activity north of the Quito-Guayllabamba basin started about 1 Ma with the "pre-Mojanda" edifice, which is one of the oldest of the current Ecuadorian arc together with Viejo Cayambe volcano. After an apparent quiescence period of ~ 500 kyr, the arc development continued between ~ 500 and 150 ka with the rapid construction of Cusín, Mojanda, Fuya Fuya, Cushnirumi and Nevado Cayambe volcanoes. The construction of Imbabura and Cubilche volcanoes could have occurred more recently, at least since ~ 55 ka, whereas the summit domes of Fuya Fuya and Huarmi dome complex were emplaced about 30 ka, at the beginning of the LGM period (Clapperton 1990). Taita Imbabura and Nevado Cayambe volcanoes were still active during the Holocene (Le Pennec et al. 2011; Samaniego et al. 1998), and the Cuicocha caldera-forming eruption occurred at 3 ka (Hillebrandt 1989).

Highest volcanic output rates are obtained for volcanoes constructed over time periods shorter than 100 kyr by sporadic eruptive pulses, whereas lowest rates are calculated over longer time periods that include quiescence phases. In Ecuador, eruptive rates range between < 0.2 and 3.6 ± 2.1 km^3/kyr. During quiescence periods, edifice morphologies are altered by various physical and chemical erosion processes depending on the age and degree of weathering of rocks. Youngest and unconsolidated deposits are rapidly transported by water circulation and surface processes, dismantled on unstable flanks, and altered by the leaching of the surface of fresh rocks, during their first ~ 200 kyr of exposure. Older and already eroded volcanoes seem mainly dismantled by slower physical processes, such as crustal faults activity and glacial-interglacial alternating periods.

The spatial distribution of the Ecuadorian volcanoes seems to be related to the slab flexure geometry, the tectonic activity and the presence of the Carnegie Ridge at depth (e.g., Gutscher et al. 1999a; Monzier et al. 1999; Yepes et al. 2016; Bablon et al. 2019). Although output rates calculated for individual volcanoes do not show any correlation with geodynamics, the number of volcanoes and their volume is significantly higher in front of the Carnegie Ridge. The subduction of the Carnegie Ridge could therefore increase the magma productivity rate at depth. Through time, the geochemistry of Mojanda magmas changes from the ~ 1 Ma calc-alkaline lava flows to younger products depleted in the most incompatible elements, as previously described for Cayambe (Samaniego et al. 2002, 2005) and Pichincha (Robin et al. 2010; Samaniego et al. 2010) volcanoes. More generally, the geochemical signature of magmas seems related to a heterogeneous mantle wedge, mainly metasomatized by hydrous fluids in the southern termination of the arc, and by siliceous melts north of the Grijalva fracture zone, closer to the Carnegie Ridge (Ancellin et al. 2017; Narvaez et al. 2018). These results provide new temporal constraints for the Quaternary arc development of northern Ecuador, and we envision that they can help to better document the relationship between volcanic activity, the edifices morphology and the geodynamic settings.

Acknowledgments The authors are grateful to Pablo Grosse, an anonymous reviewer and the associate editor for their constructive comments and useful suggestions that helped us to improve the clarity of this paper. We wish to thank the Instituto Geofísico (Escuela Politécnica Nacional) of Quito and the Institut de Recherche pour le Développement (IRD) for their support during field work and sampling. We are particularly grateful to Daniel Andrade and Alexandra Alvarado for their samples from Imbabura (IMB71), Cubilche (IMB54A) and Fuya Fuya (G-0001), as well as Valérie Godard for having manufactured all the thin sections. This study was financially supported by the INSU CNRS TelluS Aleas ([INSU 2016-ALEAS]) and IRD programs, through the Laboratoire Mixte International (LMI) project entitled "Séismes et Volcans dans les Andes du Nord" ([2012-16 LMI SVAN IRD]), and by the French Government Laboratory of Excellence initiative n°ANR-10-LABX-0006, the Région Auvergne and the European Regional Development Fund. This is LGMT contribution number 154 and Laboratory of Excellence ClerVolc contribution number 388.

References

Almeida M (2016) Estudio Petrográfico y Geoquímico del Volcán Cotacachi - Provincia de Imbabura. Ecuador, EPN, Quito

Alvarado A, Audin L, Nocquet JM, Lagreulet S, Segovia M, Font Y, Lamarque G, Yepes H, Mothes P, Rolandone F, Jarrín P, Quidelleur X (2014) Active tectonics in Quito, Ecuador, assessed by geomorphological studies, GPS data, and crustal seismicity. Tectonics 33:67–83. https://doi.org/10.1002/2012TC003224

Alvarado A, Audin L, Nocquet JM, Jaillard E, Mothes P, Jarrín P, Segovia M, Rolandone F, Cisneros D (2016) Partitioning of oblique convergence in the Northern Andes subduction zone: migration history and the present-day boundary of the North Andean Sliver in Ecuador. Tectonics 35:1048–1065. https://doi.org/10.1002/2016TC004117

Ancellin M-A, Samaniego P, Vlastélic I, Nauret F, Gannoun A, Hidalgo S (2017) Across-arc versus along-arc Sr-Nd-Pb isotope variations in the Ecuadorian volcanic arc. Geochem Geophys Geosyst 18:1163–1188. https://doi.org/10.1002/2016GC006679

Andrade Varela D (2009) The influence of active tectonics on the structural development and flank collapse of Ecuadorian arc volcanoes. Université Blaise Pascal, Clermont-Ferrand II

Andrade SD, van Wyk de Vries B, Robin C (2019) Imbabura volcano (Ecuador): the influence of dipping-substrata on the structural development of composite volcanoes during strike-slip faulting. J Volcanol Geotherm Res. https://doi.org/10.1016/j.jvolgeores.2018.11.017

Aspden JA, McCourt WJ, Brook M (1987) Geometrical control of subduction-related magmatism: the Mesozoic and Cenozoic plutonic history of Western Colombia. J Geol Soc 144:893–905

Bablon M (2018) Reconstruction de l'histoire des volcans de l'arc équatorien : contraintes pour l'évolution chronologique de l'arc andin et pour l'évaluation du risque volcanique. Univ. Paris-Sud, Université Paris-Saclay

Bablon M, Quidelleur X, Samaniego P, Le Pennec J-L, Lahitte P, Liorzou C, Bustillos JE, Hidalgo S (2018) Eruptive chronology of Tungurahua volcano (Ecuador) revisited based on new K Ar ages

and geomorphological reconstructions. J Volcanol Geotherm Res 357:378–398. https://doi.org/10.1016/j.jvolgeores.2018.05.007

Bablon M, Quidelleur X, Samaniego P, Le Pennec J-L, Audin L, Baize S, Jomard H, Liorzou C, Hidalgo S, Alvarado A (2019) Interactions between volcanism and geodynamics in the southern termination of the Ecuadorian arc. Tectonophysics 751:54–72. https://doi.org/10.1016/j.tecto.2018.12.010

Bacon CR, Lanphere MA (2006) Eruptive history and geochronology of Mount Mazama and the Crater Lake region, Oregon. Geol Soc Am Bull 118:1331–1359

Baize S, Audin L, Winter T, Alvarado A, Pilatasig Moreno L, Taipe M, Reyes P, Kauffmann P, Yepes H (2015) Paleoseismology and tectonic geomorphology of the Pallatanga fault (Central Ecuador), a major structure of the South-American crust. Geomorphology 237: 14–28. https://doi.org/10.1016/j.geomorph.2014.02.030

Baize S, Audin L, Alvarado A, Champenois J (2016) Earthquake fault segmentation in the Central Andes, Ecuador. Extended Abstract, 7th International INQUA Meeting on Paleoseismology, Active Tectonics and Archaeoseismology, Crestone, Colorado, USA

Barberi F, Coltelli M, Ferrara G, Innocenti F, Navarro JM, Santacroce R (1988) Plio-quaternary volcanism in Ecuador. Geochemical Magazine 125:1–14

Bernard B, Andrade D (2011) Volcanes Cuaternarios del Ecuador Continental. Map 1:500000

Bigazzi G, Coltelli M, Hadler NJC, Araya AMO, Oddone M, Salazar E (1992) Obsidian bearing lava flows and pre-Columbian artifacts from the Ecuadorian Andes: first new multidisciplinary data. J S Am Earth Sci 6:21–32. https://doi.org/10.1016/0895-9811(92)90014-P

Bluth GJ, Kump LR (1994) Lithologic and climatologic controls of river chemistry. Geochim Cosmochim Acta 58:2341–2359

Boland MP, Pilatasig LF, Ibandango CE, McCourt WJ, Aspden JA, Hughes RA, Beate B (2000) PRODEMINCA Report No. 10: Geology of the Western Cordillera between 0°-1°N. CODIGEM-Brit Geol Survey, Quito-Ecuador

Bourdon E, Eissen J-P, Monzier M, Robin C, Martin H, Cotten J, Hall ML (2002) Adakite-like lavas from Antisana volcano (Ecuador): evidence for slab melt metasomatism beneath the Andean Northern Volcanic Zone. J Petrol 43:199–217

Bourdon E, Eissen JP, Gutscher MA, Monzier M, Hall ML, Cotten J (2003) Magmatic response to early aseismic ridge subduction: the Ecuadorian margin case (South America). Earth Planet Sci Lett 205: 123–128

Bourdon E, Samaniego P, Monzier M, Robin C, Eissen J-P, Martin H (2004) Dubious case for slab melting in the Northern Volcanic Zone of the Andes: comment. Geology 32:e46–e47

Bryant JA, Yogodzinski GM, Hall ML, Lewicki JL, Bailey DG (2006) Geochemical constraints on the origin of volcanic rocks from the Andean Northern Volcanic Zone, Ecuador. J Petrol 47:1147–1175. https://doi.org/10.1093/petrology/egl006

Cáceres B (2010) Actualizacion del inventario de tres casquetes glaciares del Ecuador. Université Nice

Cadier E, Villacís M, Garcés A, Lhuissier P, Maishincho L, Laval R, Paredes D, Cáceres B, Francou B (2007) Variations of a low latitude Andean glacier according to global and local climate variations: first results. Glacier Hydrology (selected papers from sessions at the IAHS Assembly in Foz do Iguaçu, Brazil, 2005)

Cassignol C, Gillot P-Y (1982) Range and effectiveness of unspiked potassium-argon dating: experimental groundwork and application. In: Odin GS (ed) Numerical Dating in Stratigraphy. John Wiley & Sons, New York, pp 159–179

Chiaradia M, Müntener O, Beate B, Fontignie D (2009) Adakite-like volcanism of Ecuador: lower crust magmatic evolution and recycling. Contrib Mineral Petrol 158:563–588. https://doi.org/10.1007/s00410-009-0397-2

Clapperton CM (1990) Glacial and volcanic geomorphology of the Chimborazo-Carihuairazo Massif, Ecuadorian Andes. Trans R Soc Edinb Earth Sci 81:91–116. https://doi.org/10.1017/S0263593300005174

Cotten J, Le Dez A, Bau M, Caroff M, Maury RC, Dulski P, Fourcade S, Bohn M, Brousse R (1995) Origin of anomalous rare-earth element and yttrium enrichments in subaerially exposed basalts: evidence from French Polynesia. Chem Geol 119:115–138

Crisp JA (1984) Rates of magma emplacement and volcanic output. J Volcanol Geotherm Res 20:177–211

DeMets C, Gordon RG, Argus DF (2010) Geologically current plate motions. Geophys J Int 181:1–80. https://doi.org/10.1111/j.1365-246X.2009.04491.x

Drummond MS, Defant MJ (1990) A model for Trondhjemite-Tonalite-Dacite genesis and crustal growth via slab melting: Archean to modern comparisons. J Geophys Res Solid Earth 95:21503–21521

Dupré B, Dessert C, Oliva P, Goddéris Y, Viers J, François L, Millot R, Gaillardet J (2003) Rivers, chemical weathering and Earth's climate. Compt Rendus Geosci 335:1141–1160. https://doi.org/10.1016/j.crte.2003.09.015

Egüez A, Alvarado A, Yepes H, Machette MN, Costa C, Dart RL (2003) Database and map of quaternary faults and folds of Ecuador and its offshore regions (No. USGS Open-File Report 03289).

Erlund EJ, Cashman KV, Wallace PJ, Pioli L, Rosi M, Johnson E, Granados HD (2010) Compositional evolution of magma from Parícutin Volcano, Mexico: the tephra record. J Volcanol Geotherm Res 197:167–187. https://doi.org/10.1016/j.jvolgeores.2009.09.015

Feeley TC, Davidson JP (1994) Petrology of calc-alkaline lavas at Volcán Ollagüe and the origin of compositional diversity at Central Andean Stratovolcanoes. J Petrol 35:1295–1340

Frey HM, Lange RA, Hall CM, Delgado-Granados H (2004) Magma eruption rates constrained by 40Ar/39Ar chronology and GIS for the Ceboruco-San Pedro volcanic field, western Mexico. Geol Soc Am Bull 116:259–276. https://doi.org/10.1130/B25321.1

Gaillardet J, Dupré B, Louvat P, Allègre CJ (1999) Global silicate weathering and CO_2 consumption rates deduced from the chemistry of large rivers. Chemical Geology (Isotope Geoscience Section) 159:3–30

Garrison JM, Davidson JP (2003) Dubious case for slab melting in the Northern volcanic zone of the Andes. Geology 31:565–568

Garrison JM, Sims KWW, Yogodzinski GM, Escobar RD, Scott S, Mothes P, Hall ML, Ramon P (2018) Shallow-level differentiation of phonolitic lavas from Sumaco Volcano, Ecuador. Contributions to Mineralogy and Petrology 173. https://doi.org/10.1007/s00410-017-1431-4, 1, 19

Germa A, Quidelleur X, Gillot PY, Tchilinguirian P (2010) Volcanic evolution of the back-arc Pleistocene Payun Matru volcanic field (Argentina). J S Am Earth Sci 29:717–730. https://doi.org/10.1016/j.jsames.2010.01.002

Germa A, Quidelleur X, Lahitte P, Labanieh S, Chauvel C (2011) The K-Ar Cassignol-Gillot technique applied to western Martinique lavas: a record of Lesser Antilles arc activity from 2 Ma to Mount Pelée volcanism. Quat Geochronol 6:341–355. https://doi.org/10.1016/j.quageo.2011.02.001

Germa A, Lahitte P, Quidelleur X (2015) Construction and destruction of Mont Pelée volcano: volumes and rates constrained from a geomorphological model of evolution: construction and destruction of Mont Pelée. J Geophys Res Earth Surf 120:1206–1226. https://doi.org/10.1002/2014JF003355

Gillot P-Y, Hildenbrand A, Lefèvre J-C, Albore-Livadie C (2006) The K/Ar dating method: principle, analytical techniques, and application to Holocene volcanic eruptions in Southern Italy. Acta Vulcanol 18: 55–66

Gíslason SR, Arnorsson S, Armannsson H (1996) Chemical weathering of basalt in Southwest Iceland; effects of runoff, age of rocks and vegetative/glacial cover. Am J Sci 296:837–907. https://doi.org/10.2475/ajs.296.8.837

Grosse P, Orihashi Y, Guzmán SR, Sumino H, Nagao K (2018) Eruptive history of Incahuasi, Falso Azufre and El Cóndor Quaternary composite volcanoes, southern Central Andes. Bull Volcanol 80:1–26. https://doi.org/10.1007/s00445-018-1221-5

Gutscher M-A, Malavieille J, Lallemand S, Collot J-Y (1999a) Tectonic segmentation of the North Andean margin: impact of the Carnegie Ridge collision. Earth Planet Sci Lett 168:255–270

Gutscher M-A, Olivet J-L, Aslanian D, Eissen J-P, Maury R (1999b) The "lost Inca Plateau": cause of flat subduction beneath Peru? Earth Planet Sci Lett 171:335–341

Hall ML, Beate B (1991) Geografía y medio ambiente. El Volcanism o Plio-Cuaternario en los Andes del Ecuador:5–18

Hall ML, Mothes PA (1997) Origin and age of the Upper Cangahua Formation, Tumbaco Valley (Ecuador). Presented at the Suelos volcánicos endurecidos (Quito, diciembre 1996). Mem III Symp Intern ORSTOM, EPN, Instituto Geofisico, Ecuador, Quito, Ecuador, 19–28

Hall ML, Mothes P (2008) The rhyolitic-andesitic eruptive history of Cotopaxi volcano, Ecuador. Bull Volcanol 70:675–702. https://doi.org/10.1007/s00445-007-0161-2

Hall ML, Wood CA (1985) Volcano-tectonic segmentation of the northern Andes. Geology 13:203–207

Hall ML, Robin C, Beate B, Mothes P, Monzier M (1999) Tungurahua Volcano, Ecuador: structure, eruptive history and hazards. J Volcanol Geotherm Res 91:1–21

Hall ML, Samaniego P, Le Pennec JL, Johnson JB (2008) Ecuadorian Andes volcanism: a review of Late Pliocene to present activity. J Volcanol Geotherm Res 176:1–6. https://doi.org/10.1016/j.jvolgeores.2008.06.012

Hall ML, Mothes PA, Samaniego P, Militzer A, Beate B, Ramón P, Robin C (2017) Antisana volcano: a representative andesitic volcano of the eastern cordillera of Ecuador: petrography, chemistry, tephra and glacial stratigraphy. J S Am Earth Sci 73:50–64. https://doi.org/10.1016/j.jsames.2016.11.005

Hallet B, Hunter L, Bogen J (1996) Rates of erosion and sediment evacuation by glaciers: a review of field data and their implications. Glob Planet Chang 12:213–235

Harford CL, Pringle MS, Sparks RSJ, Young SR (2002) The volcanic evolution of Montserrat using $^{40}Ar/^{39}Ar$ geochronology. Geol Soc Lond Mem 21:93–113. https://doi.org/10.1144/GSL.MEM.2002.021.01.05

Hawkesworth C, George R, Turner S, Zellmer G (2004) Time scales of magmatic processes. Earth Planet Sci Lett 218:1–16. https://doi.org/10.1016/S0012-821X(03)00634-4

Hidalgo S (2006) Les interactions entre magmas calco-alcalins "classiques" et adakitiques : exemple du complexe volcanique Atacazo-Ninahuilca (Equateur). Université Blaise Pascal, Clermont-Ferrand II

Hidalgo S, Monzier M, Martin H, Chazot G, Eissen J-P, Cotten J (2007) Adakitic magmas in the Ecuadorian volcanic front: petrogenesis of the Iliniza volcanic complex (Ecuador). J Volcanol Geotherm Res 159:366–392. https://doi.org/10.1016/j.jvolgeores.2006.07.007

Hidalgo S, Gerbe MC, Martin H, Samaniego P, Bourdon E (2012) Role of crustal and slab components in the Northern Volcanic Zone of the Andes (Ecuador) constrained by Sr-Nd-O isotopes. Lithos 132-133:180–192. https://doi.org/10.1016/j.lithos.2011.11.019

Hildreth W, Lanphere MA (1994) Potassium-argon geochronology of a basalt-andesite-dacite arc system: the Mount Adams volcanic field, Cascade Range of southern Washington. Geol Soc Am Bull 106:1413–1429

Hildreth W, Fierstein J, Lanphere M (2003a) Eruptive history and geochronology of the Mount Baker volcanic field, Washington. Geol Soc Am Bull 115:729–764

Hildreth W, Lanphere MA, Fierstein J (2003b) Geochronology and eruptive history of the Katmai volcanic cluster, Alaska Peninsula. Earth Planet Sci Lett 214:93–114. https://doi.org/10.1016/S0012-821X(03)00321-2

Hillebrandt C (1989) Estudio geovolcanológico del complejo volcánico Cuicocha-Cotacachi y sus aplicaciones, Provincia de Imbabura. EPN, Quito. pp. 214

Hora JM, Singer BS, Worner G (2007) Volcano evolution and eruptive flux on the thick crust of the Andean Central Volcanic Zone: $^{40}Ar/^{39}Ar$ constraints from Volcan Parinacota, Chile. Geol Soc Am Bull 119:343–362. https://doi.org/10.1130/B25954.1

Jaillard E, Lapierre H, Ordonez M, Alava JT, Amortegui A, Vanmelle J (2009) Accreted oceanic terranes in Ecuador: southern edge of the Caribbean Plate? Geol Soc Lond Spec Publ 328:469–485. https://doi.org/10.1144/SP328.19

James DE (1971) Plate tectonic model for the evolution of the Central Andes. Geol Soc Am Bull 82:3325–3346

Karátson D, Telbisz T, Wörner G (2012) Erosion rates and erosion patterns of Neogene to Quaternary stratovolcanoes in the Western Cordillera of the Central Andes: an SRTM DEM based analysis. Geomorphology 139-140:122–135. https://doi.org/10.1016/j.geomorph.2011.10.010

Kendrick E, Bevis M, Smalley R, Brooks B, Vargas RB, Lauría E, Fortes LPS (2003) The Nazca-South America Euler vector and its rate of change. J S Am Earth Sci 16:125–131. https://doi.org/10.1016/S0895-9811(03)00028-2

Kennedy MJ, Chadwick OA, Vitousek PM, Derry LA, Hendricks DM (1998) Changing sources of base cations during ecosystem development, Hawaiian Islands. Geology 26(11):1015–1018. https://doi.org/10.1130/0091-7613(1998)026<1015:CSOBCD>2.3.CO;2

Klemetti EW, Grunder AL (2008) Volcanic evolution of Volcán Aucanquilcha: a long-lived dacite volcano in the Central Andes of northern Chile. Bull Volcanol 70:633–650. https://doi.org/10.1007/s00445-007-0158-x

Lahitte P, Samper A, Quidelleur X (2012) DEM-based reconstruction of southern Basse-Terre volcanoes (Guadeloupe archipelago, FWI): contribution to the Lesser Antilles Arc construction rates and magma production. Geomorphology 136:148–164. https://doi.org/10.1016/j.geomorph.2011.04.008

Lavenu A, Noblet C, Bonhomme MG, Egüez A, Dugas F, Vivier G (1992) New K-Ar age dates of Neogene and Quaternary volcanic rocks from the Ecuadorian Andes: implications for the relationship between sedimentation, volcanism, and tectonics. J S Am Earth Sci 5:309–320

Le Friant A, Harford CL, Deplus C, Boudon G, Sparks RSJ, Herd RA, Komorowski JC (2004) Geomorphological evolution of Montserrat (West Indies): importance of flank collapse and erosional processes. J Geol Soc 161:147–160

Le Pennec JL, Ruiz AG, Eissen JP, Hall ML, Fornari M (2011) Identifying potentially active volcanoes in the Andes: radiometric evidence for late Pleistocene-early Holocene eruptions at Volcán Imbabura, Ecuador. J Volcanol Geotherm Res 206:121–135. https://doi.org/10.1016/j.jvolgeores.2011.06.002

Lewis-Kenedi CB, Lange RA, Hall CM, Delgado-Granados H (2005) The eruptive history of the Tequila volcanic field, western Mexico: ages, volumes, and relative proportions of lava types. Bull Volcanol 67:391–414. https://doi.org/10.1007/s00445-004-0377-3

Litherland M, Aspden JA, Egüez A (1993) Mapa geologico de la República del Ecuador. Map 1:1 000 000

Louvat P, Allègre CJ (1997) Present denudation rates on the island of Reunion determined by river geochemistry: basalt weathering and mass budget between chemical and mechanical erosions. Geochim Cosmochim Acta 61:3645–3669

Martin H (1999) Adakitic magmas: modern analogues of Archaean granitoids. Lithos 46:411–429

Martin H, Moyen J-F, Guitreau M, Blichert-Toft J, Le Pennec J-L (2014) Why Archaean TTG cannot be generated by MORB melting in subduction zones. Lithos 198-199:1–13. https://doi.org/10.1016/j.lithos.2014.02.017

Meybeck M (1987) Global chemical weathering of surficial rocks estimated from river dissolved loads. Am J Sci 287:401–428

Monzier M, Robin C, Hall ML, Cotten J, Samaniego P (1999) Geochemistry and tectonics at the southern termination of the Northern Volcanic Zone (Riobamba volcanoes, Ecuador); preliminary results. Presented at the Fourth ISAG, Goettingen (Germany)

Narvaez DF, Rose-Koga EF, Samaniego P, Koga KT, Hidalgo S (2018) Constraining magma sources using primitive olivine-hosted melt inclusions from Puñalica and Sangay volcanoes (Ecuador). Contrib Mineral Petrol 173:10–25. https://doi.org/10.1007/s00410-018-1508-8

Newhall C, Solidum RU (2018) Volcanic hazard communication at Pinatubo from 1991 to 2015. Observing the volcano world: Volcano crisis communication. Book Series: Advances in Volcanology:189–203

Nocquet J-M, Villegas-Lanza JC, Chlieh M, Mothes PA, Rolandone F, Jarrin P, Cisneros D, Alvarado A, Audin L, Bondoux F, Martin X, Font Y, Régnier M, Vallée M, Tran T, Beauval C, Maguiña Mendoza JM, Martinez W, Tavera H, Yepes H (2014) Motion of continental slivers and creeping subduction in the northern Andes. Nat Geosci 7: 287–291. https://doi.org/10.1038/ngeo2099

Opdyke ND, Hall M, Mejia V, Huang K, Foster DA (2006) Time-averaged field at the equator: results from Ecuador. Geochemistry, Geophysics, Geosystems 7. https://doi.org/10.1029/2005GC001221

Ownby S, Delgado Granados H, Lange RA, Hall CM (2007) Volcán Tancítaro, Michoacán, Mexico, $^{40}Ar/^{39}Ar$ constraints on its history of sector collapse. J Volcanol Geotherm Res 161:1–14. https://doi.org/10.1016/j.jvolgeores.2006.10.009

Peccerillo A, Taylor SR (1976) Geochemistry of Eocene calc-alkaline volcanic rocks from the Kastamonu area, northern Turkey. Contrib Mineral Petrol 58:63–81

Pindell JL, Kennan L (2009) Tectonic evolution of the Gulf of Mexico, Caribbean and northern South America in the mantle reference frame: an update. Geol Soc Lond, Spec Publ 328:11–55. https://doi.org/10.1144/SP328.1

Presley TK, Sinton JM, Pringle M (1997) Postshield volcanism and catastrophic mass wasting of the Waianae Volcano, Oahu, Hawaii. Bull Volcanol 58:597–616

Rad S, Rivé K, Allègre CJ (2011) Weathering regime associated with subsurface circulation on volcanic islands. Aquat Geochem 17: 221–241. https://doi.org/10.1007/s10498-011-9122-7

Rad S, Rivé K, Vittecoq B, Cerdan O, Allègre CJ (2013) Chemical weathering and erosion rates in the Lesser Antilles: an overview in Guadeloupe, Martinique and Dominica. J S Am Earth Sci 45:331–344. https://doi.org/10.1016/j.jsames.2013.03.004

Rampino MR, Self S, Fairbridge RW (1979) Can rapid climatic change cause volcanic eruptions? Science 206:826–829

Ricci J, Lahitte P, Quidelleur X (2015a) Construction and destruction rates of volcanoes within tropical environment: examples from the Basse-Terre Island (Guadeloupe, Lesser Antilles). Geomorphology 228:597–607. https://doi.org/10.1016/j.geomorph.2014.10.002

Ricci J, Quidelleur X, Lahitte P (2015b) Volcanic evolution of central Basse-Terre Island revisited on the basis of new geochronology and geomorphology data. Bull Volcanol:77 https://doi.org/10.1007/s00445-015-0970-7

Robin C, Hall ML, Jimenez M, Monzier M, Escobar P (1997) Mojanda volcanic complex (Ecuador): development of two adjacent contemporaneous volcanoes with contrasting eruptive styles and magmatic suites. J S Am Earth Sci 10:345–359

Robin C, Eissen J-P, Samaniego P, Martin H, Hall M, Cotten J (2009) Evolution of the late Pleistocene Mojanda-Fuya Fuya volcanic complex (Ecuador), by progressive adakitic involvement in mantle magma sources. Bull Volcanol 71:233–258. https://doi.org/10.1007/s00445008-0219-9

Robin C, Samaniego P, Le Pennec J-L, Fornari M, Mothes P, van der Plicht J (2010) New radiometric and petrological constraints on the evolution of the Pichincha volcanic complex (Ecuador). Bull Volcanol 72:1109–1129. https://doi.org/10.1007/s00445-010-0389-0

Roverato M, Larrea P, Casado I, Mulas M, Béjar G, Bowman L (2018) Characterization of the Cubilche debris avalanche deposit, a controversial case from the northern Andes, Ecuador. J Volcanol Geotherm Res 360:22–35

Ruddiman WF (2001) Earth's climate: past and future. W.H. Freeman & Sons, New York

Ruiz AG (2003) Estudio Geovolcanológico del Complejo Volcánico Imbabura. Escuela Politécnica Nacional, Quito

Salvany T, Lahitte P, Nativel P, Gillot P-Y (2012) Geomorphic evolution of the Piton des Neiges volcano (Réunion Island, Indian Ocean): competition between volcanic construction and erosion since 1.4 Ma. Geomorphology 136:132–147. https://doi.org/10.1016/j.geomorph.2011.06.009

Samaniego P, Monzier M, Robin C, Hall ML (1998) Late Holocene eruptive activity at Nevado Cayambe Volcano, Ecuador. Bull Volcanol 59:451–459

Samaniego P, Martin H, Robin C, Monzier M (2002) Transition from calc-alkalic to adakitic magmatism at Cayambe volcano, Ecuador: insights into slab melts and mantle wedge interactions. Geology 30: 967–970

Samaniego P, Martin H, Monzier M, Robin C, Fornari M, Eissen J-P, Cotten J (2005) Temporal evolution of magmatism in the Northern Volcanic Zone of the Andes: the geology and petrology of Cayambe Volcanic Complex (Ecuador). J Petrol 46:2225–2252. https://doi.org/10.1093/petrology/egi053

Samaniego P, Robin C, Chazot G, Bourdon E, Cotten J (2010) Evolving metasomatic agent in the Northern Andean subduction zone, deduced from magma composition of the long-lived Pichincha volcanic complex (Ecuador). Contrib Mineral Petrol 160:239–260. https://doi.org/10.1007/s00410-009-0475-5

Samaniego P, Barba D, Robin C, Fornari M, Bernard B (2012) Eruptive history of Chimborazo volcano (Ecuador): a large, ice-capped and hazardous compound volcano in the Northern Andes. J Volcanol Geotherm Res 221-222:33–51. https://doi.org/10.1016/j.jvolgeores.2012.01.014

Samaniego P, Rivera M, Mariño J, Guillou H, Liorzou C, Zerathe S, Delgado R, Valderrama P, Scao V (2016) The eruptive chronology of the Ampato-Sabancaya volcanic complex (Southern Peru). J Volcanol Geotherm Res 323:110–128. https://doi.org/10.1016/j.jvolgeores.2016.04.038

Samper A, Quidelleur X, Lahitte P, Mollex D (2007) Timing of effusive volcanism and collapse events within an oceanic arc island: Basse-Terre, Guadeloupe archipelago (Lesser Antilles Arc). Earth Planet Sci Lett 258:175–191. https://doi.org/10.1016/j.epsl.2007.03.030

Samper A, Quidelleur X, Komorowski J-C, Lahitte P, Boudon G (2009) Effusive history of the Grande Découverte Volcanic Complex, southern Basse-Terre (Guadeloupe, French West Indies) from new K-Ar Cassignol-Gillot ages. J Volcanol Geotherm Res 187:117–130. https://doi.org/10.1016/j.jvolgeores.2009.08.016

Schiano P, Monzier M, Eissen J-P, Martin H, Koga KT (2010) Simple mixing as the major control of the evolution of volcanic suites in the Ecuadorian Andes. Contrib Mineral Petrol 160:297–312. https://doi.org/10.1007/s00410-009-0478-2

Singer BS, Jicha BR, Harper MA, Naranjo JA, Lara LE, Moreno-Roa H (2008) Eruptive history, geochronology, and magmatic evolution of the Puyehue-Cordon Caulle volcanic complex, Chile. Geol Soc Am Bull 120:599–618. https://doi.org/10.1130/B26276.1

Sun S-s, McDonough WF (1989) Chemical and isotopic systematics of oceanic basalts: implications for mantle composition and processes. Geological Society, London, Special Publications 42:313–345. https://doi.org/10.1144/GSL.SP.1989.042.01.19

Taylor A, Blum JD (1995) Relation between soil age and silicate weathering rates determined from the chemical evolution of a glacial chronosequence. Geology 23:979–982

Thouret J-C, Finizola A, Fornari M, Legeley-Padovani A, Suni J, Frechen M (2001) Geology of El Misti volcano near the city of Arequipa, Peru. Geol Soc Am Bull 113:1593–1610

Tibaldi A, Rovida A, Corazzato C (2007) Late Quaternary kinematics, slip-rate and segmentation of a major Cordillera-parallel transcurrent fault: the Cayambe-Afiladores-Sibundoy system, NW South America. J Struct Geol 29:664–680. https://doi.org/10.1016/j.jsg.2006.11.008

Trenkamp R, Kellogg JN, Freymueller JT, Mora HP (2002) Wide plate margin deformation, southern Central America and northwestern South America, CASA GPS observations. J S Am Earth Sci 15:157–171

Vance D, Teagle DAH, Foster GL (2009) Variable Quaternary chemical weathering fluxes and imbalances in marine geochemical budgets. Nature 458:493–496. https://doi.org/10.1038/nature07828

White SM, Crisp JA, Spera FJ (2006) Long-term volumetric eruption rates and magma budgets. Geochem Geophys Geosyst 7. https://doi.org/10.1029/2005GC001002

Yepes H, Audin L, Alvarado A, Beauval C, Aguilar J, Font Y, Cotton F (2016) A new view for the geodynamics of Ecuador: implication in seismogenic source definition and seismic hazard assessment. Tectonics 35:1249–1279. https://doi.org/10.1002/2015TC003941

Zellmer GF, Edmonds M, Straub SM (2015) Volatiles in subduction zone magmatism. Geol Soc Lond, Spec Publ 410:1–17. https://doi.org/10.1144/SP410.13